

1 **Inputs and processes affecting the distribution of particulate** 2 **iron in the North Atlantic along the GEOVIDE (GEOTRACES** 3 **GA01) section**

4
5
6 Arthur Gourain^{1,2}, H el ene Planquette¹, Marie Cheize^{1,3}, Nolwenn Lemaitre^{1,4}, Jan-Lukas
7 Menzel Barraqueta^{5, 6}, Rachel Shelley^{1, 7}, Pascale Lherminier⁸ and G eraldine Sarthou¹

8
9 1-UMR 6539/LEMAR/IUEM, CNRS, UBO, IRD, Ifremer, Technop ole Brest Iroise, Place Nicolas Copernic,
10 29280 Plouzan e, France

11 2- now at Ocean Sciences Department, School of Environmental Sciences, University of Liverpool, Liverpool,
12 L69 3GP, United Kingdom

13 3- now at Ifremer, Centre de Brest, G eosciences Marines, Laboratoire des Cycles G eochimiques (LCG), 29280
14 Plouzan e, France

15 4- now at Department of Earth Sciences, Institute of Geochemistry and Petrology, ETH-Z urich, Z urich,
16 Switzerland

17 5- GEOMAR, Helmholtz Centre for Ocean Research Kiel, Wischhofstra e 1-3, 24148 Kiel, Germany

18 6- now at Department of Earth Sciences, Stellenbosch University, Stellenbosch, 7600, South Africa

19 7- now at Earth, Ocean and Atmospheric Science, Florida State University, Tallahassee, Florida, 32310, USA

20 8- Ifremer, Univ. Brest, CNRS, IRD, Laboratoire d'Oc eanographie Physique et Spatiale (LOPS), IUEM, F-
21 29280, Plouzan e, France

22
23 *Correspondence to: helene.planquette@univ-brest.fr*

24 25 **Abstract**

26 The aim of the GEOVIDE cruise (May-June 2014, R/V *Pourquoi Pas?*) was to provide a better understanding of
27 trace metal biogeochemical cycles in the North Atlantic Ocean. As marine particles play a key role in the global
28 biogeochemical cycle of trace elements in the ocean, we discuss the distribution of particulate iron (PFe), in
29 relation to the distribution of particulate aluminium (PAI), manganese (PMn) and phosphorus (PP). Overall, 32
30 full vertical profiles were collected for trace metal analyses, representing more than 500 samples. This resolution
31 provides a solid basis for assessing concentration distributions, elemental ratios, size-fractionation, and adsorptive
32 scavenging processes in key areas of the thermohaline overturning circulation. Total particulate iron
33 concentrations ranged from as low as 9 pmol L⁻¹ in surface waters of the Labrador Sea to 304 nmol L⁻¹ near the
34 Iberian margin, while median PFe concentrations of 1.15 nmol L⁻¹ were measured over the sub-euphotic ocean
35 interior.

36 Within the Iberian Abyssal Plain, the ratio of PFe to PAI was identical to the continental crust molar ratio (0.21
37 mol mol⁻¹), indicating the important influence of crustal particles in the water column. Overall, the lithogenic

38 component explained more than 87% of PFe variance along the section. Within the Irminger and Labrador basins,
39 the formation of biogenic particles led to an increase of the PFe/PAI ratio (up to 0.64 mol mol⁻¹) compared to the
40 continental crust ratio. Continental margins induce high concentrations of particulate trace elements within the
41 surrounding water masses (up to 10 nmol L⁻¹ of PFe). For example, horizontal advection of PFe was visible more
42 than 250 km away from the Iberian margin. Additionally, several benthic nepheloid layers were observed more
43 than 200 m above the seafloor along the transect, especially in the Icelandic, Irminger and Labrador basins,
44 suspending particles with high PFe content of up to 89 nmol L⁻¹.

45

46 **1. Introduction**

47 Particles play a key role in the ocean where they drive the residence time of most elements (Jeandel and Oelkers,
48 2015), and strongly influence the global biogeochemistry of macro- and micro-nutrients including iron (Milne et
49 al., 2017). In the surface ocean, biological activity produces biogenic suspended matter through planktonic
50 organisms, while atmospheric deposition (Baker et al., 2013; Jickells et al., 2005), riverine discharge (Aguilar-
51 Islas et al., 2013; Berger et al., 2008; Ussher et al., 2004) or ice-melting (Hawkings et al., 2014; Lannuzel et al.,
52 2011, 2014) deliver mostly lithogenic derived particles to surface waters. These particulate inputs are highly
53 variable, both spatially and seasonally, in the world's oceans. At depth, benthic and shelf sediment resuspension
54 (e.g. Aguilar-Islas et al., 2013; Cullen et al., 2009; Elrod et al., 2004; Fitzwater et al., 2000; Hwang et al., 2010;
55 Lam et al., 2015; Lam and Bishop, 2008; McCave and Hall, 2002), and hydrothermal activity (Elderfield and
56 Schultz, 1996; Lam et al., 2012; Tagliabue et al., 2010, 2017; Trefry et al., 1985), provides important amounts of
57 particles to the water column. Moreover, authigenic particles can be produced *in-situ* by aggregation of colloids
58 (Bergquist et al., 2007) or oxidation processes (Bishop and Fleisher, 1987; Collier and Edmond, 1984). Thus,
59 oceanic particles result from a complex combination of these different sources and processes (Lam et al., 2015).
60 In the upper water column, the total iron pool is dominated by marine particles (Radic et al., 2011) which strongly
61 interact with the dissolved pool (e.g. Ellwood et al., 2014). Indeed, dissolved iron can be scavenged onto particles
62 (Gerringa et al., 2015; Rijkenberg et al., 2014), incorporated into biogenic particles (Berger et al., 2008) or
63 produced by remineralisation of particles (Dehairs et al., 2008; Sarthou et al., 2008). Interestingly, the concept of
64 “reversible scavenging” of iron (i.e. release at depth of dissolved iron previously scavenged onto particles) has
65 been advocated recently (Abadie et al., 2017; Dutay et al., 2015; Jeandel and Oelkers, 2015; Labatut et al., 2014),
66 while other studies reveal distinct dissolution processes of inorganic particulate iron (e.g. Oelkers et al., 2012;
67 Cheize et al., 2018). Slow dissolution of particulate iron at margins has also been evoked as a continuous fertilizer
68 of primary production and should be considered as a source of dissolved iron (e.g. Jeandel et al., 2011; Jeandel
69 and Oelkers, 2015; Lam and Bishop, 2008). Within or below the mixed layer, the rates of regeneration processes
70 can also impact the bioavailable pool of iron, among other trace metals (e.g. Ellwood et al., 2014; Nuester et al.,
71 2014). However, the rates of these processes are not yet fully constrained. The study of particulate iron is thus
72 essential to better constrain its marine biogeochemical cycle. Interest has grown in this subject over the last 10
73 years, in particular (e.g. Abadie et al., 2017; Bishop and Biscaye, 1982; Collier and Edmond, 1984; Frew et al.,
74 2006; Lam et al., 2012; Milne et al., 2017; Planquette et al., 2011, 2013; Sherrell et al., 1998) and, to our
75 knowledge, only two studies have been performed on an ocean-wide scale: the GA03 GEOTRACES North
76 Atlantic Zonal Transect (Lam et al., 2015;
77 Ohnemus and Lam, 2015) and the GP16 GEOTRACES Pacific Transect (Lam et al., 2017; Lee et al., 2017).

78 Within this global context, this paper presents the particulate iron distribution of the North Atlantic Ocean, along
79 the GEOTRACES GA01 section (GEOVIDE), and discusses the various sources and processes affecting
80 particulate iron (PFe) distribution, using particulate aluminium (PAI), phosphorus (PP) or manganese (PMn)
81 distributions to support our conclusions.
82

83 **2. Methods**

84 2.1. Study area

85 Particulate samples were collected at 32 stations during the GEOVIDE (GEOTRACES GA01 section) cruise
86 between May and June 2014 aboard the R/V *Pourquoi Pas?* in the North Atlantic Ocean (Sarhou et al., 2018).
87 The sampling spanned several biogeochemical provinces (Figure 1), starting over the Iberian margin (IM, Stations
88 2, 4 and 1), and proceeding to the Iberian Abyssal Plain (IAP, Stations 11 to 17), the Western European Basin
89 (WEB, Station 19 to Station 29) and the Icelandic Basin (IcB, Stations 32 to 36). Then, samples were collected
90 above the Reykjanes Ridge (RR, Station 38), in the Irminger Basin (IrB, Stations 40 to 60), close to the Greenland
91 shelf (GS, Stations 53, 56 and 61), the Labrador Basin (LB, Stations 63 to 77) and finally close the Newfoundland
92 shelf (NS, Station 78) (Figure 1). The North Atlantic is characterized by a complex circulation (briefly described
93 in section 3.1 and in detail by Zunino et al. (2017) and García-Ibáñez et al. (2015)) and is one of the most
94 productive regions of the global ocean (Martin et al., 1993; Sanders et al., 2014).
95

96 2.2. Sampling

97 Samples were collected using the French GEOTRACES clean rosette, equipped with twenty-two 12 L GO-FLO
98 bottles (two bottles were leaking and were not deployed during the cruise). GO-FLO bottles (General Oceanic's)
99 were initially cleaned in the home laboratory (LEMAR) following the GEOTRACES procedures (Cutter and
100 Bruland, 2012). The rosette was deployed on a 14 mm Kevlar cable with a dedicated, custom-designed clean
101 winch. Immediately after recovery, the GO-FLO bottles were individually covered at each end with plastic bags
102 to minimize contamination. Bottles were then transferred into a clean container (class-100) for sampling. On each
103 cast, nutrient and/or salinity samples were taken to check potential leakage of the GO-FLO bottles.
104

105 Filters were cleaned following the GEOTRACES protocols (<http://www.geotraces.org/images/Cookbook.pdf>)
106 and kept in acid-cleaned 1 L LDPE bottles (Nalgene) filled with ultrapure water (Milli-Q, resistivity of 18.2 MΩ
107 cm) until use. All filters were 25 mm diameter in order to optimize the signal over the filter blank, except at the
108 surface depth where 47 mm diameter filters were used. The filters were mounted on acid-cleaned polysulfone
109 filter holders (Nalgene™). Prior to filtration, the GO-FLO bottles were shaken three times, as recommended in
110 the GEOTRACES cookbook to avoid settling of particles in the lower part of the bottle. GO-FLO bottles were
111 pressurized to < 8 psi with 0.2 μm filtered nitrogen gas (N₂, Air Liquide). Seawater was then filtered directly
112 through paired filters (Pall Gelman Supor™ 0.45 μm polyetersulfone, and Millipore mixed ester cellulose MF 5
113 μm) mounted in Swinnex polypropylene filter holders (Millipore), following Planquette and Sherrell (2012) inside
114 the clean container. Filtration was operated until the bottle was empty or until the filter clogged; the volume
115 filtered ranged from 2 L for surface samples to 11 L within the water column. After filtration, filter holders were
116 disconnected from the GO-FLO bottles and a gentle vacuum was applied using a syringe in order to remove any

117 residual water under a laminar flow hood. Filters were then removed from the filter holders with plastic tweezers
118 (which were rinsed with Milli-Q between samples). Most of the remaining seawater was removed via ‘sipping’
119 by capillary action, when placing the non-sampled side of the filter onto a clean 47 mm supor filter. Each filter
120 pair was then placed in an acid-cleaned polystyrene PetriSlide (Millipore), double bagged, and finally stored at -
121 20 °C until analysis at LEMAR. Between casts, filter holders were thoroughly rinsed with Milli-Q, placed in an
122 acid bath (5% Trace metal grade HCl) for 24 hours, then rinsed with Milli-Q.

123 At each station, process blanks were collected as follows: 2 L of a deep (1000 m) and a shallow (40 m) seawater
124 sample were first filtered through a 0.2 µm pore size capsule filter (Pall Gelman Acropak 200) mounted on to the
125 outlet of the GO-FLO bottle before passing through the particle sampling filter, which was attached directly to
126 the swinnex filter holder.

127

128 2.3. Analytical methods

129 In the home laboratory, sample handling was performed inside a clean room (Class 100). All solutions were
130 prepared using ultrapure water (Milli-Q) and all plasticware had been acid-cleaned before use. Frozen filters,
131 collected within the mixed layer or within nepheloid layers, were first cut in half using a ceramic blade: one filter
132 half was dedicated to total digestion (see below), while the other half was archived at -20 °C for SEM analyses or
133 acid leaching of “labile” metals following Berger et al. (2008) method (to be published separately).

134 Filters were digested following the method described in Planquette and Sherrell (2012). Filters were placed on
135 the inner wall of acid-clean 15 mL PFA vials (Savillex™), and 2 mL of a solution containing 2.9 mol L⁻¹
136 hydrofluoric acid (HF, suprapur grade, Merck) and 8 mol L⁻¹ nitric acid (HNO₃, Ultrapur grade, Merck) was added
137 to each vial. Vials were then closed and refluxed at 130 °C on a hot plate for 4 hours, after which the filters were
138 removed. After cooling, the digest solution was evaporated at 110 °C to near dryness. Then, 400 µL of
139 concentrated HNO₃ (Ultrapur grade, Merck) was added, and the solution was re-evaporated at 110 °C. Finally,
140 the obtained residue was dissolved with 3 mL of 0.8 mol L⁻¹ HNO₃ (Ultrapure grade, Merck). This archived
141 solution was transferred to an acid cleaned 15 mL polypropylene centrifuge tube (Corning®) and stored at 4 °C
142 until analyses.

143 All analyses were performed on a sector field inductively coupled plasma mass spectrometer (SF-ICP-MS
144 Element 2, Thermo-Fisher Scientific). Samples were diluted by a factor of 7 on the day of analysis in acid-washed
145 13 mm (outer diameter) rounded bottom, polypropylene centrifuge tubes (VWR) with 0.8 mol L⁻¹ HNO₃ (Ultrapur
146 grade, Merck) spiked with 1 µg L⁻¹ of indium (¹¹⁵In) solution in order to monitor the instrument drift. Samples
147 were introduced with a PFA-ST nebulizer connected to a quartz cyclonic spray chamber (Elemental Scientific
148 Incorporated, Omaha, NE) via a modified SC-Fast introduction system consisting of an SC-2 autosampler, a six-
149 port valve and a vacuum-rinsing pump. The autosampler was contained under a HEPA filtered unit (Elemental
150 Scientific). Two 6-point, matrix-matched multi-element standard curves with concentrations bracketing the range
151 of the samples were run at the beginning, the middle and the end of each analytical run. Analytical replicates were
152 made every 10 samples, while accuracy was determined by performing digestions of the certified reference
153 material BCR-414 (plankton, Community Bureau of Reference, Commission of the European Communities),
154 PACS-3 and MESS-4 (marine sediments, National Research Council Canada), following the same protocol used
155 for the samples. Recoveries were typically within 10% of the certified values (and within the error of the data,
156 taken from replicate measurements, Table 1). Once all data were normalized to an ¹¹⁵In internal standard and

157 quantified using an external standard curve, the dilution factor of the total digestion was accounted for. The
158 elemental concentrations were obtained per filter (pmol/filter) and were then process blank-corrected. Finally,
159 pmol/filter values were divided by the volume of water filtered through stacked filters.
160 Total concentrations (sum of small size fraction (0.45-5 µm) and large (>5 µm) size fraction) of particulate trace
161 elements are reported in Table S1.

162

163 2.4. Positive matrix factorisation

164 Positive Matrix Factorisation (PMF) was run to characterise the main factors influencing the particulate trace
165 element variance along the GEOVIDE section. In addition to PFe, PAI, PMn, and PP, nine additional elements
166 were included in the PMF: yttrium (Y), barium (Ba), lead (Pb), thorium (Th), titanium (Ti), vanadium (V), cobalt
167 (Co), copper (Cu) and zinc (Zn). The PMF was conducted on samples where all elements were above their
168 detection limits; after selection, 445 of the 549 existing data points were used. Analyses were performed using
169 the PMF software, EPA PMF 5.0, developed by the USA Environmental Protection Agency (EPA). Three to six
170 factor models were run on the data. The configuration that provided the lowest error estimation (i.e. was the most
171 reliable) was the four factor model. To ensure stability, this model was run 100 times. After displacement, error
172 estimation and bootstrap error estimation, the model was recognised as stable.

173

174 2.5. Derived and ancillary parameters

175 To investigate the proportion of lithogenic iron within the bulk particulate iron, we used the Upper Continental
176 Crust (UCC) Fe/Al molar ratio (0.21) of Taylor and McLennan (1995) to calculate the lithogenic components of
177 particles (%PFelitho) following Eq. (1):

178

$$179 \quad \%PFelitho = 100 * \left(\frac{PAI}{PFe} \right)_{sample} * \left(\frac{PFe}{PAI} \right)_{UCCratio} \quad (1)$$

180

181 The non-lithogenic PFe is obtained using Eq. (2):

182

$$183 \quad \%PFenon_litho = 100 - \%PFelitho \quad (2)$$

184

185 Note that while the %PFelitho and %PFenon-litho proxies are interesting tools to evaluate the importance of lithogenic
186 and non-lithogenic (either biogenic or authigenic) fraction, they have to be used carefully, as the spatial and
187 temporal variation of the lithogenic component ratios may involve uncertainties of the estimated fraction value.

188 In addition to PAI, PMn can be used as a tracer of inputs from shelf resuspension (Lam and Bishop, 2008), using
189 a percentage of sedimentary inputs “%bulk sediment inputs” estimated according to the following equation:

$$190 \quad \%bulksedimentPMn = 100 * \left(\frac{PAI}{PMn} \right)_{sample} * \left(\frac{PMn}{PAI} \right)_{UCCratio} \quad (3)$$

191 with PAI/PMn being the ratio from the GEOVIDE samples and the PMn/PAI being the UCC value (0.0034; Taylor
192 and McLennan, 1995).

193 This proxy can be a good indicator of sediment resuspension. We assume that particles newly resuspended in the
194 water column will have the same PMn/PAI ratio as the UCC ratio, leading to a “%bulk sediment Mn” of 100%.
195 This proxy assumes homogeneity of the sediment PMn/PAI ratio throughout the GEOVIDE section. However,
196 this may not be the case at every station. In consequence, this proxy should only be used to identify new benthic
197 resuspension at specific locations; inter-comparison between several locations may not be appropriate. When a
198 sample presents a “%bulk sediment Mn” greater than 100%, we have assigned a maximum value of 100%. As the
199 Mn cycle can also be influenced by biotic uptake (e.g. Peers and Price, 2004; Sunda and Huntsman, 1983), this
200 proxy is only used at depths where biologic activity was negligible (i.e. below 150m depth).

201 Potential temperature (θ°), salinity (S), and transmissometry data were retrieved from the CTD sensors (CTD
202 SBE911 equipped with a SBE43).

203

204

205 **3. Results**

206 *3.1. Hydrography setting*

207 Here, we briefly describe the hydrography encountered during the GEOVIDE section (Figure 2) as a thorough
208 description is available in García-Ibáñez et al. (2015). At the start of the section, the warm and salty Mediterranean
209 Water (MW, $S = 36.50$, $\theta^\circ = 11.7$ °C) was sampled between 600 and 1700 m in the Iberian Abyssal Plain (IAP).
210 MW resulted from the mixing between the Mediterranean Overflow Water (MOW) plume coming from the
211 Mediterranean Sea and local waters. Surface water above the Iberian Shelf was characterised by low salinity ($S =$
212 34.95) at station 2 and 4 compared to surrounding water masses. Close to the sea floor of the Iberian Abyssal
213 Basin, the North East Atlantic Deep Water (NEADW, $S = 34.89$, $\theta^\circ = 2.0$ °C) spread northward. The North
214 Atlantic Central Water (NACW, $S > 35.60$, $\theta^\circ > 12.3$ °C) was the warmest water mass of the transect and was
215 observed in the subsurface layer of the Western European Basin and Iberian Abyssal Plain. An old Labrador Sea
216 Water (LSW, $S = 34.87$, $\theta^\circ = 3.0$ °C) flowed inside the Western European and Icelandic Basins, between 1000
217 and 2500m depth.

218 In the Icelandic Basin, below the old LSW, the Iceland-Scotland Overflow Water (ISOW, $S = 34.98$, $\theta^\circ = 2.6$ °C)
219 spread along the Reykjanes Ridge slope. This cold water, originating from the Arctic, led to the formation of
220 NEADW after mixing with surrounding waters. North Atlantic hydrography was impacted by the northward
221 flowing of the North Atlantic Current (NAC), which carried warm and salty waters from the subtropical area. Due
222 to air-sea interactions and mixing with surrounding water, the NACW is cooled and freshened in the subpolar
223 gyre and is transformed in Subpolar Mode Water (SPMW). The formation of SPMW inside the Icelandic and
224 Irminger Basins leads to the formation of regional mode waters: the Iceland Subpolar Mode Water (IcSPMW, S
225 $= 35.2$, $\theta^\circ = 8.0$ °C) and the Irminger Subpolar Mode Water (IrSPMW, $S = 35.01$, $\theta^\circ = 5.0$ °C), respectively.
226 IcSPMW was a relatively warm water mass with potential temperature up to 7 °C (García-Ibáñez et al., 2015).
227 Another branch of the NAC mixed with Labrador Current waters to form the relatively fresh SubArctic
228 Intermediate Water (SAIW, $S = < 34.8$, 4.5 °C $< \theta^\circ < 6$ °C).

229 The Irminger Basin is a complex area with a multitude of water masses. In the middle of the basin, an old LSW,
230 formed one year before (Straneo et al., 2003), spread between 500 and 1200 m depth. Close to the bottom, the

231 Denmark Strait Overflow Water (DSOW, $S = 34.91$) flowed across the basin. Greenland coastal waters were
232 characterised by low salinity values, down to $S = 33$. The strong East Greenland Current (EGC) flowed southward
233 along the Greenland shelf in the Irminger Basin. At the southern tip of Greenland, this current enters the Labrador
234 Basin along the west coast of Greenland and followed the outline of the basin until the Newfoundland shelf. In
235 the Labrador Basin, the deep convection of SPMW at 2000 m was involved in the formation of the LSW ($S =$
236 34.9 , $\theta = 3.0^\circ\text{C}$) (García-Ibáñez et al., 2015; Yashayaev and Loder, 2009). Above the Newfoundland Shelf,
237 surface waters were affected by discharge from rivers and ice-melting and characterised by extremely low salinity
238 for open ocean waters, below 32 in the first 15 meters.

239 3.2. Section overview

240 Total particulate concentrations spanned a large range of concentrations from below detection (Table 1) to 304
241 nmol L^{-1} for PFe, 1544 nmol L^{-1} for PAI, 3.5 nmol L^{-1} for PMn and 402 nmol L^{-1} for PP. The ranges of
242 concentrations are comparable to other studies recently published (Table 2).

243 Along the section, PFe, PAI, and PMn were predominantly found ($> 90\%$) in particles larger than $5 \mu\text{m}$, except
244 in surface waters, reflecting a more heterogenous pattern, where $9 \pm 8.6\%$ of PFe, $10.9 \pm 15.4\%$ of PAI and 32.8
245 $\pm 16.6\%$ of PMn, $38.8 \pm 8.6\%$ of PP were hosted by smaller particles ($0.45\text{-}5 \mu\text{m}$). Data are shown in Figure 3.

246

247 3.3. Open Ocean stations: from the Iberian Abyssal Plain to the Labrador Basin

248 This concerns all stations from station 11 to 77, with the exception of stations 53, 56 and 61 which were sampled
249 close to the Greenland coast (Figure 1). Particulate iron concentration profiles showed identical patterns at all the
250 open ocean stations encountered along the section. Median PFe was low at 0.25 nmol L^{-1} within the first 100 m
251 and steadily increased with depth. However, at two stations, elevated concentrations were determined in the upper
252 100 m, up to 4.4 nmol L^{-1} at station 77 at 40 m depth and 7 nmol L^{-1} at station 63 between 70 and 100 m depth.
253 PFe concentrations gradually increased with depth, with a median PFe of 1.74 nmol L^{-1} below 1000m. Close to
254 the seafloor of some stations (26, 29, 32, 34, 49, 60, and 71), high concentrations of PFe were observed, up to 88
255 nmol L^{-1} (station 71 at 3736 m). These high PFe values were associated with low beam transmissometry values \leq
256 97% .

257 Particulate aluminium and manganese profiles were similar to PFe profiles, with low concentrations measured in
258 the first 100 m (1.88 nmol L^{-1} and 55 pmol L^{-1} , respectively) which increased towards the seafloor. Close to the
259 seafloor, high concentrations were determined at the same stations cited above for PFe, with a maximum of 264
260 nmol L^{-1} and 3.5 nmol L^{-1} for PAI and PMn respectively at station 71 (supplementary Table S1). Highest
261 particulate phosphorus concentrations were in the uppermost 50 m, with a median value of 66 nmol L^{-1} . Below
262 200 m depth PP concentrations decreased to values below 10 nmol L^{-1} . Inter-basins differences were observed
263 within surface samples, with median PP concentration being higher in the Irminger Basin (127 nmol L^{-1}) than in
264 the Iberian Abyssal Plain (28 nmol L^{-1}) (Figure 3).

265 Finally, above the Reykjanes Ridge, PP, PMn, PAI and PFe concentrations were in the same range as the
266 surrounding open ocean stations. However, close to the seafloor, high concentrations were measured, with PFe,

267 PAI, and PMn reaching 16.2 nmol L⁻¹, 28.8 nmol L⁻¹, and 0.51 nmol L⁻¹ at 1354 m depth, respectively (Figure 3
268 and Table S1).

269

270 3.4. Margins and Shelves: Iberian Margin (stations 1 to 4), Greenland coast (stations 53, 56
271 and 61) and Newfoundland Shelf (station 78)

272

273 The Iberian margin was characterised by low beam transmissometry values at station 2 (88 % at 140 m depth,
274 Figure 4a) suggesting high particle concentrations. Particulate iron concentrations varied from 0.02 nmol L⁻¹ to
275 304 nmol L⁻¹. Within the first 50 m, PFe concentrations decreased towards the shelf break where PFe dropped
276 from 2.53 nmol L⁻¹ (station 2) to 0.8 nmol L⁻¹ (Station 1). At all three stations, PFe concentrations increased with
277 depth and reached a maximum close to the seafloor. For example, 300 nmol L⁻¹ of PFe was determined at 138.5
278 m depth at station 2. Lithogenic tracers, such as PAI or PMn, presented similar profiles to PFe with concentrations
279 ranging from 0.11 and 1544 nmol L⁻¹, and from below detection limit to 2.51 nmol L⁻¹, respectively (Figure 3,
280 Table S1). Total particulate phosphorus concentrations were relatively low in surface waters ranging from values
281 below detection to 38 nmol L⁻¹; concentrations decreased with depth and were less than 0.7 nmol L⁻¹ below 1000
282 m depth.

283 In the vicinity of the Greenland shelf, PFe concentrations had a high median value of 10.8 nmol L⁻¹ and were
284 associated with high median PAI and PMn concentrations of 32.3 nmol L⁻¹ and 0.44 nmol L⁻¹, respectively.
285 Concentrations of PP were high at the surface with a value of 197 nmol L⁻¹ at 25 m depth of station 61. Then, PP
286 concentrations decreased strongly, to less than 30 nmol L⁻¹ below 100 meters depth. Furthermore, beam
287 transmissometry values in surface waters at these three stations, were the lowest of the entire section, with values
288 below 85 % (Figure 4a).

289 Close to the Newfoundland margin, surface waters displayed a small load of particulate trace metals as PFe, PAI,
290 and PMn concentrations were below 0.8 nmol L⁻¹, 2 nmol L⁻¹, and 0.15 nmol L⁻¹, respectively. Then, close to the
291 bottom of station 78, at 371 m depth, beam transmissometry values dropped to 94 % (Figure 4a) and were
292 associated with extremely high concentrations of PFe = 168 nmol L⁻¹, PAI = 559 nmol L⁻¹, and PMn = 2 nmol L⁻¹.
293 Total PP concentrations in the first 50 m ranged from 35 to 97 nmol L⁻¹. Below 50 m, PP remained relatively
294 high with values up to 16 nmol L⁻¹ throughout the water column. (Figure 3 and Table S1).

295

296 **4. Discussion**

297 Our goal was to investigate mechanisms that drive the distribution of PFe in the North Atlantic, in particular the
298 different routes of supply and removal. Possible sources of PFe include lateral advection offshore from margins,
299 atmospheric inputs, continental run-off, melting glaciers and icebergs, resuspended sediments, hydrothermal
300 inputs and biological uptake. Removal processes include remineralization, dissolution processes and sediment
301 burial.

302 In the following sections, we examine each of these sources and processes, explore the evidence for their relative
303 importance, and use compositional data to estimate the particle types and host phases for iron and associated
304 elements.

305 4.1. Analysis of the principal factors controlling variance: near-ubiquitous influence of crustal
306 particles in the water column

307 Positive matrix factorisation analysis (Figure 5) was undertaken on the entire dataset, in consequence, the factors
308 described below are highly influenced by the major variations of particulate element concentrations (usually at
309 the interfaces, i.e. margin, seafloor, surface layer). The first factor is characterised by lithogenic elements,
310 representing 86.8 % of the variance of PFe, 75.8 % of PAI and 90.5 % of PTi. The second factor is correlated with
311 both Mn and Pb and explains no less than 76.5 % and 77.0 % of their respective variances. Ohnemus and Lam
312 (2015) observed this co-relation between manganese and lead particles and explained it by the co-transport on
313 Mn-oxides (Boyle et al., 2005). The formation of barite explains the third factor and constrained 87.7 % of the Ba
314 variance in the studied regions. Biogenic barite accumulation within the mesopelagic layer is related to bacterial
315 activity and remineralisation of biogenic material (Lemaitre et al., 2018a). A biogenic component is the fourth
316 factor and explained most of PP variance, 83.7 %. The micronutrient trace metals, copper, cobalt and zinc, had
317 more than a quarter of their variances influenced by this factor. Note that the biogenic contribution to PFe and
318 other trace elements will be discussed in another paper (Planquette et al., in prep).

319 These results indicate that along the GA01 section, PFe distributions were predominantly controlled by lithogenic
320 material and to a smaller extent by remineralisation processes (PMF, factor 3 = 4.1 %). This does not rule out
321 some biogenic influences on PFe distribution, especially in the surface, but its contribution is most likely obscured
322 by the high lithogenic contribution.

323 To further investigate the influence of crustal material on the distribution of PFe, it is instructive to examine the
324 distribution of the PFe to PAI molar ratio, and the resulting %PFe_{litho} (see section 2.6 for definition of this
325 parameter) along the section (Figure 6). Overall, the estimated lithogenic contribution to PFe varies from 25 %
326 (west of the Irminger Basin, station 60, 950 m depth) to 100 % at stations located within the Western European
327 Basin. Note that 100% of estimated lithogenic PFe does not necessary mean that biogenic particles are absent;
328 they may just be masked by the dominance of lithogenic particles. Important inter-basin variations are observed
329 along the section (Figure 6). The IAP and WEB displayed high median values of the proxy %PFe_{litho}, 90 % (Figure
330 6b); this could be linked to the lateral advection of iron rich lithogenic particles sourced from the Iberian margin
331 and to atmospheric inputs (Shelley et al., 2017). Then, between stations 26 and 29, the %PFe_{litho} proxy values
332 dramatically decreased, and reached values less than 55 % in the Iceland, Irminger and the Labrador basins (Figure
333 6b). This feature is likely associated with the presence of the Sub-Arctic Front located between 49.5 and 51 °N
334 latitude and 23.5 and 22 °W longitude (Zunino et al., 2017). Indeed, this front which separates cold and fresh
335 water of subpolar origin from warm and salty water of subtropical origin was clearly identifiable by the steep
336 gradient of the isohalines between station 26 and 29; salinity dropping from 35.34 to 35.01 (Figure 2). Lower
337 %PFe_{litho} proxy values, could be associated with higher proportions of PFe from biogenic origin, especially in the
338 case of the LSW.

339

340 4.2. Tracking the different inputs of particulate iron

341 4.2.1. Inputs at margins: Iberian, Greenland and Newfoundland

342 Inputs of iron from continental margin sediments supporting the high productivity found in shallow coastal regions
343 have been demonstrated in the past (e.g. Cullen et al. 2009, Elrod et al. 2004, Jeandel et al. 2011, Ussher et al.
344 2007) and sometimes, were shown to be advected at great distances from the coast (e.g. Lam and Bishop, 2008).
345 In the following section, we will investigate these possible sources in proximity to the different margins
346 encountered.

347

348 *The Iberian margin*

349 The Iberian margin was an important source of lithogenic-derived iron-rich particles to the Atlantic Ocean during
350 GEOVIDE; shelf resuspension impacts were perceptible up to 280 km from the margin (Station 11) in the Iberian
351 Abyssal Plain (Figure 8).

352 On the shelf, at station 2, high sediment resuspension resulted in the low beam transmissometry value (87.6 %) at
353 the immediate vicinity of the seafloor (153 m depth). This sediment resuspension led to an extensive input of
354 lithogenic particles within the water column associated with high concentrations of PFe (304 nmol L⁻¹), PAI (1500
355 nmol L⁻¹), and PMn (2.5 nmol L⁻¹) (Figure 3, Table S1). Moreover, 100 % of PFe was estimated to have a
356 lithogenic origin (Figure 8b) while 100 % of the PMn was estimated to be the result of a recent sediment
357 resuspension according to the %PFe_{litho} and “%bulk sediment Mn” proxies (Figure 8b and c), confirming the
358 resuspended particle input. In addition, ADCP data acquired during GEOVIDE (Zunino et al., 2017) and several
359 other studies have reported an intense current spreading northward coming from the Straits of Gibraltar and
360 Mediterranean Sea, leading to the strong resuspension of benthic sediments above the Iberian Shelf (e.g. Biscaye
361 and Eittrheim, 1977, Eittrheim et al., 1976, McCave and Hall, 2002, Spinrad et al., 1983).

362 At distance from the shelf, within the Iberian Abyssal Plain, an important lateral advection of PFe from the margin
363 was observable (Figure 8a). These lateral inputs occurred at two depth ranges: between 400 and 1000 m as seen
364 at stations 4 and 1, with PFe concentrations reaching 4 nmol L⁻¹, and between 2500 m and the bottom (3575 m)
365 of station 1, with PFe concentrations reaching 3.5 nmol L⁻¹. While 100 % of PFe had a lithogenic signature, the
366 sedimentary source input estimation decreased, between 40 % and 90 % of the PMn (Figure 8b). Transport of
367 lithogenic particles was observable until station 11 (12.2°W) at 2500 m where PFe concentration was 7.74 nmol
368 L⁻¹ and 60 % of PMn had a sedimentary origin (Figure 4). It is noteworthy that no increase in PFe, PMn or PAI
369 was observed between 500 and 2000 m depth, where the MOW spreads (García-Ibáñez et al., 2015). This is
370 consistent with the observed dissolved iron (DFe) concentrations (Tonnard et al., 2018, this issue), yet in contrast
371 to dissolved aluminium (DAI) concentrations (Menzel-Barraqueta et al., 2018, this issue) which were high in the
372 MOW, and with the study of Ohnemus and Lam (2015) that reported a maximum PFe concentration at 695 m
373 depth associated with the particle-rich Mediterranean Overflow Water (Eittrheim et al., 1976) in the IAP. However,
374 their station was located further south of our station 1. The shallower inputs observed at stations 1 and 4 could
375 therefore be attributed to sediment resuspension from the Iberian margin and nepheloid layer at depth for station
376 1.

377 Surface coastal waters of the Iberian Shelf are impacted by the runoff for the Tagus River, which is characterised
378 by high suspended matter discharges, ranging between 0.4 to 1 × 10⁶ tons yr⁻¹, and with a high anthropogenic
379 trace element signature (Jouanneau et al., 1998). During the GEOVIDE section, the freshwater input was
380 observable at stations 1, 2 and 4 in the first 20 m; salinity was below 35.2 while surrounding water masses had

381 salinity up to 35.7. Within the freshwater plume, particulate concentrations were high at station 2 with PFe of 1.83
382 nmol L⁻¹. Further away from the coast, the particulate concentrations remained low at 20m depth, with PFe, PAI,
383 and PMn concentrations of 0.77 nmol L⁻¹, 3.5 nmol L⁻¹, and 0.04 nmol L⁻¹, respectively at station 1. The low
384 expansion of the Tagus plume is likely due to the rapid settling of suspended matter. Indeed, our coastal station 2
385 was located approximately 50 km from the Iberian coast, whereas the surface particle load can only be observed
386 at a maximum distance of 30 km from the Tagus estuary (Jouanneau et al., 1998). Overall, the Iberian margin
387 appears to be an important source of lithogenic-derived iron rich particles to the Atlantic Ocean.

388

389 *South Greenland*

390 During GEOVIDE, the Greenland shelves were a source of particulate-rich meteoric water leading to a transfer
391 of DFe to PFe by enhanced biological activity. Indeed, both East (station 53) and West (station 61) Greenland
392 shelves had high concentration of particles (beam transmissometry of 83 %, Figure 4a) and particulate trace
393 elements, reaching 22.1 nmol L⁻¹ (at 100 m depth) and 18.7 nmol L⁻¹ (at 136 m depth) of PFe, respectively. Several
394 studies have already demonstrated the importance of icebergs and sea ice melting as sources of dissolved and
395 particulate iron (e.g. van der Merwe et al., 2011a, 2011b; Planquette et al., 2011; Raiswell et al., 2008). The
396 Greenland shelf is highly influenced by external fresh water inputs such as sea-ice-melting or riverine runoff
397 (Fragoso et al., 2016), which are important sources of iron to the Greenland Shelf (Bhatia et al., 2013; Hawkings
398 et al., 2014; Statham et al., 2008). During the cruise, the relative freshwater observed ($S < 33$ psu) within the first
399 25 m of stations 53 and 61 was associated with high PFe (19 nmol L⁻¹), PAI (61 nmol L⁻¹), PMn (0.6 nmol L⁻¹)
400 and low beam transmissometry ($\leq 85\%$) (Figure 4a and Table S1). The associated particles were enriched in iron
401 compared to aluminium, as PFe/PAI ratio was 0.3 within the meteoric water plume. The high PP concentrations
402 (reaching 197 nmol L⁻¹) resulting from high biological production (Chl-a = 6.21 mg m⁻³ at 24 m at station 61),
403 induced by the supply of bioavailable dissolved iron (surface DFe of 0.79 nM at station 61) from meteoric water
404 (Raiswell et al., 2008; Statham et al., 2008; Tonnard et al. 2018), led to a transfer of DFe to the particulate phase.
405 This is in line with the finding that around 30 % PFe had a non-lithogenic origin. In addition, only 40% PMn
406 originated from resuspended sediments. Interestingly, these two proxies remained constant from the seafloor to
407 the surface (Station 49, Figure 8), with around 25 % of the PMn of sedimentary origin, which could be due to
408 important mixing occurring on the shelf. The lithogenic PFe could result from the release of PFe from Greenland
409 bedrock captured during the ice sheet formation on land.

410 The spatial extent of the off-shelf lateral transport of particles was not important on the east Greenland coast.
411 Indeed, no visible increase of particulate trace metal concentrations was visible at the first station off-shelf, station
412 60 (Figure 8), except at 1000 m depth, where a strong increase (up to 90 %) of sedimentary PMn was seen. This
413 is probably due to the East Greenland Coastal Current (EGCC) that was located at station 53 which constrained
414 these inputs while stations 56 and 60 were under the influence of another strong current, the East Greenland-
415 Irminger current (EGIC) (Zunino et al., 2017). To the west of the Greenland margin, lateral transport of particles
416 was slightly more important. Noticeable concentrations of particulate lithogenic elements were observable until
417 station 64 located 125 km away from shoreline. These particles had a decreased PFe lithogenic contribution (50
418 %) with a similar (25 %) sedimentary PMn content than closer to the margin (Figure 8b and c). The increasing
419 nature of non-lithogenic PFe is linked to the bloom in surface waters (PFe/PAI ratio of 0.30 mol mol⁻¹, PP of 197
420 nmol L⁻¹ and Chl-a concentration of 6.21 mg m⁻³ at station 61), with the gravitational settling of biogenic PFe.

421 Therefore, particles newly resuspended from Greenland sediments are an important source, representing around
422 one third of the pMn pool, combined with surface inputs such as riverine runoff and/or ice-melting that are
423 delivering particles on the shelf, and also biological production. Unlike the Iberian shelf, the Greenland margin
424 was not an important provider of particulate metals inside the Irminger and Labrador Basins, due to the circulation
425 that constrained the extent of the margin plume.

426

427

428 *The Newfoundland Shelf*

429 Previous studies have already described the influence of fresh water on the Newfoundland shelf from the Hudson
430 Strait and/or Canadian Arctic Archipelago (Fragoso et al., 2016; Yashayaev, 2007). Yashayaev (2007) also
431 monitored strong resuspension of sediments associated with the spreading of the Labrador Current along the West
432 Labrador margin.

433 Close to the Newfoundland coastline, at station 78, high fresh water discharge (≤ 32 psu) was observed in surface
434 waters (Benetti et al., 2017). Interestingly, these freshwater signatures were not associated with elevated
435 particulate trace metal concentrations. Distance of meteoric water sources implied a long travel time for the water
436 to spread through the Labrador Basin to our sampling stations. Along the journey, particles present originally may
437 have been removed from the water column by gravitational settling.

438 The proportion of lithogenic PFe was relatively high and constant throughout the water column, with a median
439 value of 70 %. At station 78, 95 % of the PMn had a sedimentary origin close to the seafloor (371 m). The
440 spreading of the recent sediment resuspension was observable until 140 m depth where the contribution of
441 sedimentary Mn was still 51% (Figure 8c, Table S2). This could correspond to an intense nepheloid layer as
442 previously reported by Biscaye and Eittrheim (1977) (see also section 3.3.2). The high PFe concentration (184
443 nmol L⁻¹, station 78, 371 m depth, Figure 8b) associated with a high percentage of sedimentary PMn (95%)
444 observed at the bottom of this station, was therefore the result of an important resuspension of shelf sediments.
445 This was confirmed with low transmissometry values of 95 % (Figure 4a).

446

447 Along the GEOVIDE section, continental shelves provided an important load of particles to the surrounding water
448 column. The three margins sampled during GEOVIDE behaved very differently; the Iberian margin discharged
449 high quantities of lithogenic particles far from the coast while the Greenland and Newfoundland margins did not
450 reveal important PFe concentrations. Spreading of particles is tightly linked to hydrodynamic conditions, which
451 in the case of the Greenland margin, prevented long distance seeding of PFe. Moreover, each margin showed a
452 specific PFe/PAI ratio (Figure 9) indicating different composition of the resuspended particles. Resuspended
453 particles represent the composition of sediment at the margin if redox transformation of iron and aluminium are
454 considered negligible under these circumstances. Differences between margins were due to the presence of non-
455 crustal particles, either biogenic or authigenic. Biological production in surface waters and authigenic formation
456 of iron hydroxide produced particles with a higher PFe/PAI content and their export through the water column to
457 the sediment increased the PFe/PAI ratio at depth. Regions where biological production is intense such as in the
458 vicinity of Newfoundland presented higher PFe/PAI ratios of resuspended benthic particles.

459

460

4.2.2 Benthic resuspended sediments

461 Along the GEOVIDE section, Benthic nepheloid layers (BNLs) provided high concentrations of particulate trace
462 elements to the deep open ocean, contributing significantly to the total budget of iron. BNLs were observable in
463 each province, although intensities varied (Figures 3 and 10).

464 In BNLs located within the WEB, PFe concentrations reached up to 10 nmol L⁻¹ (stations 26 and 29, Figure 10a;
465 Table S1). These concentrations were lower than PFe concentrations in BNLs from the Icelandic (stations 32 and
466 34), Irminger (stations 42 and 44) and Labrador Basins (stations 68, 69 and 71), where benthic resuspension led
467 to PFe concentrations higher than 40 nmol L⁻¹, even reaching 89 nmol L⁻¹ at the bottom of station 71 (3736 m
468 depth). Moreover, in the Irminger and Labrador Basins, PFe/PAI molar ratios within BNLs were higher than the
469 ones measured within the WEB at station 26 and 29. In the Irminger Basin, PFe/PAI reached 0.4 mol mol⁻¹ (Figure
470 10b), which could reveal a mixture of lithogenic and biogenic matter that had been previously exported. This
471 feature was also observed in the Labrador Basin, with PFe/PAI ratio ranging between 0.34 and 0.44 mol mol⁻¹. In
472 contrast, BNLs sampled in the WEB clearly have a lithogenic imprint, with PFe/PAI molar ratios close to the
473 crustal one. Resuspended sediments with a non-crustal contribution seem to have higher PFe contents than
474 sediments with lithogenic characteristics. Nevertheless, interestingly all BNLs present during GEOVIDE were
475 spreading identically, with impacts observable up to 200 m above the oceanic seafloor (Figure 10), as reflected in
476 beam transmissometry values, and PFe concentrations, which returned to background levels at 200 m above the
477 seafloor. The presence of these BNLs has also been reported by Le Roy et al. (2018) using radium-226 activity.
478 Important differences of PFe intensities could also be due to different hydrographic components and topographic
479 characteristics. BNLs occur due to strong hydrographic stresses (i.e. boundary currents, benthic storms and deep
480 eddies) interacting with the ocean floor (Biscaye and Eittrheim, 1977; Eittrheim et al., 1976; Gardner et al., 2017,
481 2018). They are, by definition, highly variable geographically and temporally, but we have no physical data which
482 would allow us to investigate this hypothesis further.

483

484

4.2.3. Reykjanes Ridge inputs

485 Above the Reykjanes Ridge (Station 38), high PFe concentrations were determined, reaching 16 nmol L⁻¹ just
486 above the seafloor, while increased DFe concentrations were reported to the east of the ridge (Tonnard et al.,
487 2018, this issue). The exact sources of iron-rich particles cannot be well constrained, as they could come from
488 active hydrothermal vents or resuspension of particulate matter from new crustal matter produced at the ridge.
489 According to the oceanic circulation (Zunino et al., 2017; Garcia-Ibanez et al., 2017), hydrothermal particles could
490 have been seen in the ISOW within the Icelandic Basin. Nevertheless, at the vicinity of the ridge, scanning electron
491 microscope (SEM) analyses of our samples did reveal several biological debris and clays but not the presence of
492 iron (oxy-)hydroxide particles (supplementary figure S1), which are known to be produced close to hydrothermal
493 vents (Elderfield and Schultz, 1996). Their absence could thus indicate an absence of vents. However, data from
494 other proxies, such as helium-3, would be necessary to confirm the presence or absence of an hydrothermal source
495 close to station 38.

496

497

4.2.4. Atmospheric inputs

498 Atmospheric deposition is an important source of trace elements in surface of the open ocean (e.g. Jickells et al.,
499 2005). Atmospheric inputs, both wet and dry, were reported to be low during the GEOVIDE cruise (Menzel

500 Barraqueta et al., 2018b, this issue; Shelley et al., 2017; 2018). In fact, oceanic particle measurements in surface
501 waters along the section did not reveal high PFe or PAI concentrations. One pattern is interesting to note: the
502 surface waters of the Iberian Abyssal Plain and Western European Basin, between stations 11 and 23 presented a
503 characteristic feature with really low PFe/PAI elemental ratios, of 0.11, smaller than the UCC ratio of 0.21 (Figure
504 6a). Such low ratios have been reported in the same region by Barrett et al. (2012). One possible explanation is
505 given by Buck et al. (2010) who described Fe-depleted aerosols in this area of the North Atlantic with PFe/PAI
506 ratio below UCC ratio. However, Shelley et al. (2017) found a higher PFe/PAI ratio around 0.25 in this area (their
507 samples geoa5-6). This result, highlights some of the difficulties in linking atmospheric inputs to water column
508 data (Baker et al., 2016), and implies a probable fractionation after aerosol deposition. In addition, there is high
509 spatial and temporal variability of atmospheric deposition (Mahowald et al., 2005) and a certain degree of
510 uncertainty about the dissolution processes of atmospherically-transported particles (Bonnet and Guieu, 2004).

511

512

513

5. Conclusions

514

515 The investigation of the PFe composition of suspended particulate matter along the GEOVIDE section in the
516 North Atlantic reflects the pervasive influence of crustal particles, augmented by sedimentary inputs at margins,
517 and within benthic nepheloid layers at depths. In consequence, variance of particulate iron along the section is
518 mainly explained by lithogenic factors.

519 Resuspension of sedimentary particles from continental shelves are responsible of high particulate iron
520 concentrations within the surrounding water column and could be observed at long distances from the shelf, in
521 the case of the Iberian margin. Our results also demonstrate the impact of Arctic meteoric water on the Greenland
522 shelf, while in surface waters, the enhancement of productivity by new bioavailable iron is leading to a transfer
523 of dissolved iron to the particulate phase. Benthic nepheloid layer are providing important concentration of
524 particles to the water column; they were observed in most of the oceanic basin encountered along the GEOVIDE
525 section.

526 Overall, PFe distributions in the North Atlantic are strongly influenced by sources at its boundaries (i.e.
527 continental margins and seafloor). When combined with other datasets from the GEOTRACES program in a
528 modelling study, for example, use of this data will facilitate a greater understanding of particulate iron cycling in
529 the North Atlantic.

530

531

532

533 Acknowledgments

534 We are greatly indebted to the captain and crew of the N/O Pourquoi Pas? for their help during the GEOVIDE
535 mission and clean rosette deployment. We would like to give special thanks to Fabien Pérault and Emmanuel de
536 Saint Léger for their technical expertise, to Catherine Schmechtig for the GEOVIDE database management and
537 Greg Cutter for his guidance in setting up the new French clean sampling system. We would like to thank both
538 reviewers for constructive comments that greatly improved this manuscript. We especially would like to highlight
539 the contribution of Christian Schlosser as a reviewer.

540 We also would like to thank Reiner Schlitzer for the Ocean Data View software (ODV).
541 This work was supported by the French National Research Agency (ANR-13-BS06-0014, ANR-12-PDOC-0025-
542 01), the French National Centre for Scientific Research (CNRS-LEFE-CYBER), the LabexMER (ANR-10-
543 LABX-19), and Ifremer. It was supported for the logistic by DT-INSU and GENAVIR.

544

545 **References**

546 Abadie, C., Lacan, F., Radic, A., Pradoux, C. and Poitrasson, F.: Iron isotopes reveal distinct dissolved iron
547 sources and pathways in the intermediate versus deep Southern Ocean, *114*(5), 1–6,
548 doi:10.1073/pnas.1603107114, 2017.

549 Aguilar-Islas, A. M., Rember, R., Nishino, S., Kikuchi, T. and Itoh, M.: Partitioning and lateral transport of iron
550 to the Canada Basin, *Polar Sci.*, *7*(2), 82–99, doi:10.1016/j.polar.2012.11.001, 2013.

551 Baker, A. R., Adams, C., Bell, T. G., Jickells, T. D. and Ganzeveld, L.: Estimation of atmospheric nutrient inputs
552 to the Atlantic Ocean from 50°N to 50°S based on large-scale field sampling: Iron and other dust-associated
553 elements, *Global Biogeochem. Cycles*, *27*(3), 755–767, doi:10.1002/gbc.20062, 2013.

554 Baker, A. R., Landing, W. M., Bucciarelli, E., Cheize, M., Fietz, S., Hayes, C. T., Kadko, D., Morton, P. L.,
555 Rogan, N., Sarthou, G., Shelley, R. U., Shi, Z., Shiller, A. and van Hulten, M. M. P.: Trace element and isotope
556 deposition across the air–sea interface: progress and research needs, *Philos. Trans. R. Soc. A Math. Phys. Eng.*
557 *Sci.*, *374*(2081), 20160190, doi:10.1098/rsta.2016.0190, 2016.

558 Barrett, P. M., Resing, J. A., Buck, N. J., Buck, C. S., Landing, W. M. and Measures, C. I.: The trace element
559 composition of suspended particulate matter in the upper 1000m of the eastern North Atlantic Ocean: A16N, *Mar.*
560 *Chem.*, 142–144, 41–53, doi:10.1016/j.marchem.2012.07.006, 2012.

561 Benetti, M., Reverdin, G., Lique, C., Yashayaev, I., Holliday, N. P., Tynan, E., Torres-Valdes, S., Lherminier, P.,
562 Tréguer, P., and Sarthou, G.: Composition of freshwater in the spring of 2014 on the southern Labrador shelf and
563 slope, *Journal of Geophysical Research: Oceans*, *122*, 1102–1121, 10.1002/2016jc012244, 2017.

564 Berger, C. J. M., Lippiatt, S. M., Lawrence, M. G. and Bruland, K. W.: Application of a chemical leach technique
565 for estimating labile particulate aluminum, iron, and manganese in the Columbia River plume and coastal waters
566 off Oregon and Washington, *J. Geophys. Res.*, *113*, C00B01, doi:10.1029/2007JC004703, 2008.

567 Bergquist, B. A., Wu, J. and Boyle, E. A.: Variability in oceanic dissolved iron is dominated by the colloidal
568 fraction, *Geochim. Cosmochim. Acta*, *71*(12), 2960–2974, doi:10.1016/j.gca.2007.03.013, 2007.

569 Bhatia, M. P., Kujawinski, E. B., Das, S. B., Breier, C. F., Henderson, P. B. and Charette, M. A.: Greenland
570 meltwater as a significant and potentially bioavailable source of iron to the ocean, *Nat. Geosci.*, *6*(4), 274–278,
571 doi:10.1038/ngeo1746, 2013.

- 572 Biscaye, P. E. and Eitrem, S. L.: Suspended Particulate Loads and Transports in the Nepheloid Layer of the
573 Abyssal Atlantic Ocean, *Dev. Sedimentol.*, 23(C), 155–172, doi:10.1016/S0070-4571(08)70556-9, 1977.
- 574 Bishop, J. K. B. and Biscaye, P. E.: Chemical characterization of individual particles from the nepheloid layer in
575 the Atlantic Ocean, *Earth Planet. Sci. Lett.*, 58(2), 265–275, doi:10.1016/0012-821X(82)90199-6, 1982.
- 576 Bishop, J. K. B. and Fleisher, M. Q.: Particulate manganese dynamics in Gulf Stream warm-core rings and
577 surrounding waters of the N.W. Atlantic, *Geochim. Cosmochim. Acta*, 51(10), 2807–2825, doi:10.1016/0016-
578 7037(87)90160-8, 1987.
- 579 Bonnet, S. and Guieu C.: Dissolution of atmospheric iron in seawater, *Geophys. Res. Lett.*, 31(3), L03303,
580 doi:10.1029/2003GL018423, 2004.
- 581 Boyle, E. A., Bergquist, B. A., Kayser, R. A. and Mahowald, N.: Iron, manganese, and lead at Hawaii Ocean
582 Time-series station ALOHA: Temporal variability and an intermediate water hydrothermal plume, *Geochim.*
583 *Cosmochim. Acta*, 69(4), 933–952, doi:10.1016/j.gca.2004.07.034, 2005.
- 584 Buck, C. S., Landing, W. M., Resing, J. A. and Measures, C. I.: The solubility and deposition of aerosol Fe and
585 other trace elements in the North Atlantic Ocean: Observations from the A16N CLIVAR/CO2repeat hydrography
586 section, *Mar. Chem.*, 120(1–4), 57–70, doi:10.1016/j.marchem.2008.08.003, 2010.
- 587 Cheize, M., Planquette, H. F., Fitzsimmons, J. N., Pelleter, E., Sherrell, R. M., Lambert, C., Bucciarelli, E.,
588 Sarthou, G., Le Goff, M., Liorzou, C., Chéron, S., Viollier, E., and Gayet, N.: Contribution of resuspended
589 sedimentary particles to dissolved iron and manganese in the ocean: An experimental study, *Chemical Geology*.
590 doi: 10.1016/j.chemgeo.2018.10.003, 2018.
- 591 Collier, R. and Edmond, J.: The trace element geochemistry of marine biogenic particulate matter, *Prog.*
592 *Oceanogr.*, 13(2), 113–199, doi:10.1016/0079-6611(84)90008-9, 1984.
- 593 Cullen, J. T., Chong, M. and Ianson, D.: British columbia continental shelf as a source of dissolved iron to the
594 subarctic northeast Pacific Ocean, *Global Biogeochem. Cycles*, 23(4), 1–12, doi:10.1029/2008GB003326, 2009.
- 595 Cutter, G. A. and Bruland, K. W.: Rapid and noncontaminating sampling system for trace elements in global
596 ocean surveys, *Limnol. Oceanogr. Methods*, 10(JUNE), 425–436, doi:10.4319/lom.2012.10.425, 2012.
- 597 Dammshäuser, A., Wagener, T., Garbe-Schönberg, D. and Croot, P.: Particulate and dissolved aluminum and
598 titanium in the upper water column of the Atlantic Ocean, *Deep. Res. Part I Oceanogr. Res. Pap.*, 73, 127–139,
599 doi:10.1016/j.dsr.2012.12.002, 2013.
- 600 Dehairs, F., Jacquet, S., Savoye, N., Van Mooy, B. A. S., Buesseler, K. O., Bishop, J. K. B., Lamborg, C. H.,
601 Elskens, M., Baeyens, W., Boyd, P. W., Casciotti, K. L. and Monnin, C.: Barium in twilight zone suspended
602 matter as a potential proxy for particulate organic carbon remineralization: Results for the North Pacific, *Deep.*
603 *Res. Part II Top. Stud. Oceanogr.*, 55(14–15), 1673–1683, doi:10.1016/j.dsr2.2008.04.020, 2008.

604 Dutay, J. C., Tagliabue, A., Kriest, I. and van Hulst, M. M. P.: Modelling the role of marine particles on large
605 scale ^{231}Pa , ^{230}Th , Iron and Aluminium distributions, *Prog. Oceanogr.*, 133, 66–72,
606 doi:10.1016/j.pocean.2015.01.010, 2015.

607 Eittrich, S., Thorndike, E. M. and Sullivan, L.: Turbidity distribution in the Atlantic Ocean, *Deep. Res. Oceanogr.*
608 *Abstr.*, 23(12), 1115–1127, doi:10.1016/0011-7471(76)90888-3, 1976.

609 Elderfield, H. and Schultz, A.: Mid-Ocean Ridge Hydrothermal Fluxes and the Chemical Composition of the
610 Ocean, *Annu. Rev. Earth Planet. Sci.*, 24(1), 191–224, doi:10.1146/annurev.earth.24.1.191, 1996.

611 Ellwood, M. J., Nodder, S. D., King, A. L., Hutchins, D. A., Wilhelm, S. W. and Boyd, P. W.: Pelagic iron cycling
612 during the subtropical spring bloom, east of New Zealand, *Mar. Chem.*, 160, 18–33,
613 doi:10.1016/j.marchem.2014.01.004, 2014.

614 Elrod, V. A., Berelson, W. M., Coale, K. H. and Johnson, K. S.: The flux of iron from continental shelf sediments:
615 A missing source for global budgets, *Geophys. Res. Lett.*, 31(12), 2–5, doi:10.1029/2004GL020216, 2004.

616 Fitzwater, S. E., Johnson, K. S., Gordon, R. M., Coale, K. H. and Smith, W. O.: Trace metal concentrations in
617 the Ross Sea and their relationship with nutrients and phytoplankton growth, *Deep. Res. Part II Top. Stud.*
618 *Oceanogr.*, 47(15–16), 3159–3179, doi:10.1016/S0967-0645(00)00063-1, 2000.

619 Fragoso, G. M., Poulton, A. J., Yashayaev, I. M., Head, E. J. H., Stinchcombe, M. C. and Purdie, D. A.:
620 Biogeographical patterns and environmental controls of phytoplankton communities from contrasting
621 hydrographical zones of the Labrador Sea, *Prog. Oceanogr.*, 141, 212–226, doi:10.1016/j.pocean.2015.12.007,
622 2016.

623 Frew, R. D., Hutchins, D. A., Nodder, S., Sanudo-Wilhelmy, S., Tovar-Sanchez, A., Leblanc, K., Hare, C. E. and
624 Boyd, P. W.: Particulate iron dynamics during FeCycle in subantarctic waters southeast of New Zealand, *Global*
625 *Biogeochem. Cycles*, 20(1), 1–15, doi:10.1029/2005GB002558, 2006.

626 García-Ibáñez, M. I., Pardo, P. C., Carracedo, L. I., Mercier, H., Lherminier, P., Ríos, A. F. and Pérez, F. F.:
627 Structure, transports and transformations of the water masses in the Atlantic Subpolar Gyre, *Prog. Oceanogr.*, 135,
628 18–36, doi:10.1016/j.pocean.2015.03.009, 2015.

629 Gardner, W. D., Tucholke, B. E., Richardson, M. J. and Biscaye, P. E.: Benthic storms, nepheloid layers, and
630 linkage with upper ocean dynamics in the western North Atlantic, *Mar. Geol.*, 385, 304–327,
631 doi:10.1016/j.margeo.2016.12.012, 2017.

632 Gardner, W. D., Richardson, M. J. and Mishonov, A. V.: Global assessment of benthic nepheloid layers and
633 linkage with upper ocean dynamics, *Earth Planet. Sci. Lett.*, 482, 126–134, doi:10.1016/j.epsl.2017.11.008, 2018.

634 Gerringa, L. J. A., Rijkenberg, M. J. A., Schoemann, V., Laan, P. and de Baar, H. J. W.: Organic complexation
635 of iron in the West Atlantic Ocean, *Mar. Chem.*, 177, 434–446, doi:10.1016/j.marchem.2015.04.007, 2015.

636 Hawkings, J. R., Wadham, J. L., Tranter, M., Raiswell, R., Benning, L. G., Statham, P. J., Tedstone, A., Nienow,
637 P., Lee, K. and Telling, J.: Ice sheets as a significant source of highly reactive nanoparticulate iron to the oceans,
638 *Nat. Commun.*, 5(May), 1–8, doi:10.1038/ncomms4929, 2014.

639 Hwang, J., Druffel, E. R. M. and Eglinton, T. I.: Widespread influence of resuspended sediments on oceanic
640 particulate organic carbon: Insights from radiocarbon and aluminum contents in sinking particles, *Global*
641 *Biogeochem. Cycles*, 24(4), 1–10, doi:10.1029/2010GB003802, 2010.

642 Jeandel, C. and Oelkers, E. H.: The influence of terrigenous particulate material dissolution on ocean chemistry
643 and global element cycles, *Chem. Geol.*, 395, 50–66, doi:10.1016/j.chemgeo.2014.12.001, 2015.

644 Jeandel, C., Peucker-Ehrenbrink, B., Jones, M. T., Pearce, C. R., Oelkers, E. H., Godderis, Y., Lacan, F., Aumont,
645 O. and Arsouze, T.: Ocean margins: The missing term in oceanic element budgets?, *Eos, Transactions American*
646 *Geophysical Union*, 92(26), 217–224, doi: 10.1029/2011EO260001, 2011.

647 Jickells, T. D., An, Z. S., Andersen, K. K., Baker, A. R., Bergametti, C., Brooks, N., Cao, J. J., Boyd, P. W., Duce,
648 R. A., Hunter, K. A., Kawahata, H., Kubilay, N., LaRoche, J., Liss, P. S., Mahowald, N., Prospero, J. M.,
649 Ridgwell, A. J., Tegen, I. and Torres, R.: Global iron connections between desert dust, ocean biogeochemistry,
650 and climate, *Science* (80-.), 308(5718), 67–71, doi:10.1126/science.1105959, 2005.

651 Jouanneau, J. M., Garcia, C., Oliveira, A., Rodrigues, A., Dias, J. A. and Weber, O.: Dispersal and deposition of
652 suspended sediment on the shelf off the Tagus and Sado estuaries, S.W. Portugal, *Prog. Oceanogr.*, 42(1–4), 233–
653 257, doi:10.1016/S0079-6611(98)00036-6, 1998.

654 Labatut, M., Lacan, F., Pradoux, C., Chmeleff, J., Radic, A., Murray, J. W., Poitrasson, F., Johansen, A. M., Thil,
655 F., Lacan, F., Pradoux, C., Chmeleff, J., Radic, A., Murray, J. W., Poitrasson, F., Johansen, A. M. and Thil, F.:
656 Iron sources and dissolved-particulate interactions in the seawater of the Western Equatorial Pacific, iron isotope
657 perspectives., *Global Biogeochem Cycles*, 1044–1065, doi:10.1002/2014GB004928, 2014.

658 Lam, P. J. and Bishop, J. K. B.: The continental margin is a key source of iron to the HNLC North Pacific Ocean,
659 *Geophys. Res. Lett.*, 35(7), 1–5, doi:10.1029/2008GL033294, 2008.

660 Lam, P. J., Ohnemus, D. C. and Marcus, M. A.: The speciation of marine particulate iron adjacent to active and
661 passive continental margins, *Geochim. Cosmochim. Acta*, 80, 108–124, doi:10.1016/j.gca.2011.11.044, 2012.

662 Lam, P. J., Ohnemus, D. C. and Auro, M. E.: Size-fractionated major particle composition and concentrations
663 from the US GEOTRACES North Atlantic Zonal Transect, *Deep. Res. Part II Top. Stud. Oceanogr.*, 116, 303–
664 320, doi:10.1016/j.dsr2.2014.11.020, 2015.

665 Lam, P. J., Lee, J. M., Heller, M. I., Mehic, S., Xiang, Y. and Bates, N. R.: Size-fractionated distributions of
666 suspended particle concentration and major phase composition from the U.S. GEOTRACES Eastern Pacific Zonal
667 Transect (GP16), *Mar. Chem.*, (April), 0–1, doi:10.1016/j.marchem.2017.08.013, 2017.

668 Lannuzel, D., Bowie, A. R., van der Merwe, P. C., Townsend, A. T. and Schoemann, V.: Distribution of dissolved
669 and particulate metals in Antarctic sea ice, *Mar. Chem.*, 124(1–4), 134–146, doi:10.1016/j.marchem.2011.01.004,
670 2011.

671 Lannuzel, D., Van der Merwe, P. C., Townsend, A. T. and Bowie, A. R.: Size fractionation of iron, manganese
672 and aluminium in Antarctic fast ice reveals a lithogenic origin and low iron solubility, *Mar. Chem.*, 161, 47–56,
673 doi:10.1016/j.marchem.2014.02.006, 2014.

674 Lee, J. M., Heller, M. I. and Lam, P. J.: Size distribution of particulate trace elements in the U.S. GEOTRACES
675 Eastern Pacific Zonal Transect (GP16), *Mar. Chem.*, 201(September 2017), 108–123,
676 doi:10.1016/j.marchem.2017.09.006, 2017.

677 Lemaître, N., planquette, H., Planchon, F., Sarthou, G., Jacquet, S., Garcia-Ibanez, M. I., Gourain, A., Cheize,
678 M., Monin, L., Andre, L., Laha, P., Terryn, H., and Dehairs, F.: Particulate barium tracing significant mesopelagic
679 carbon remineralisation in the North Atlantic, *Biogeosciences*, doi:10.5194/bg-15-2289-2018, 2018a.

680 Lemaître, N., Planchon, F., Planquette, H., Dehairs, F., Fonseca-Batista, D., Roukaerts, A., Deman, F., Tang, Y.,
681 Mariez, C., and Sarthou G.: High variability of export fluxes along the North Atlantic GEOTRACES section
682 GA01: Particulate organic carbon export deduced from the ^{234}Th method, *Biogeosciences*, doi:10.5194/bg-2018-
683 190, 2018b.

684 Le Roy, E., Sanial, V., Charette, M.A., Van Beek, P., Lacan, F., Jacquet, S.H., Henderson, P.B., Souhaut, M.,
685 García-Ibáñez, M.I., Jeandel, C. and Pérez, F.: The ^{226}Ra -Ba relationship in the North Atlantic during
686 GEOTRACES-GA01, *Biogeosciences*, doi:10.5194/bg-2017-478, 2018.

687 Marsay, C. M., Lam, P. J., Heller, M. I., Lee, J. M. and John, S. G.: Distribution and isotopic signature of ligand-
688 leachable particulate iron along the GEOTRACES GP16 East Pacific Zonal Transect, *Mar. Chem.*, (November
689 2016), 1–14, doi:10.1016/j.marchem.2017.07.003, 2017.

690 Martin, J. H., Fitzwater, S. E., Michael Gordon, R., Hunter, C. N. and Tanner, S. J.: Iron, primary production and
691 carbon-nitrogen flux studies during the JGOFS North Atlantic bloom experiment, *Deep. Res. Part II*, 40(1–2),
692 115–134, doi:10.1016/0967-0645(93)90009-C, 1993.

693 McCave, I. N. and Hall, I. R.: Turbidity of waters over the Northwest Iberian continental margin, *Prog. Oceanogr.*,
694 52(2–4), 299–313, doi:10.1016/S0079-6611(02)00012-5, 2002.

695 Menzel Barraqueta, J.L., Schlosser, C., Planquette, H., Gourain, A., Cheize, M., Boutorh, J., Shelley, R., Pereira
696 Contreira, L., Gledhill, M., Hopwood, M.J. and Lherminier, P.: Aluminium in the North Atlantic Ocean and the
697 Labrador Sea (GEOTRACES GA01 section): roles of continental inputs and biogenic particle removal.
698 *Biogeosciences*, 1-28, doi: 10.5194/bg-2018-39, 2018.
699

700 Menzel Barraqueta, J.-L., Klar, J. K., Gledhill, M., Schlosser, C., Shelley, R., Planquette, H., Wenzel, B.,
701 Sarthou, G., and Achterberg, E. P.: Atmospheric aerosol deposition fluxes over the Atlantic Ocean: A
702 GEOTRACES case study, *Biogeosciences Discuss.*, <https://doi.org/10.5194/bg-2018-209>, in review, 2018b.

703 Milne, A., Schlosser, C., Wake, B. D., Achterberg, E. P., Chance, R., Baker, A. R., Forryan, A. and Lohan, M.
704 C.: Particulate phases are key in controlling dissolved iron concentrations in the (sub)tropical North Atlantic,
705 *Geophys. Res. Lett.*, 44(5), 2377–2387, doi:10.1002/2016GL072314, 2017.

706 Nuester, J., Shema, S., Vermont, A., Fields, D. M. and Twining, B. S.: The regeneration of highly bioavailable
707 iron by meso- and microzooplankton, *Limnol Oceanogr*, 59(4), 1399–1409, doi:10.4319/lm.2014.59.4.1399, 2014.

708 Oelkers, E. H., Jones, M. T., Pearce, C. R., Jeandel, C., Eiriksdottir, E. S. and Gislason, S. R.: Riverine particulate
709 material dissolution in seawater and its implications for the global cycles of the elements, *Geosci.*, 344(11–12),
710 646–651, doi:10.1016/j.crte.2012.08.005, 2012.

711 Ohnemus, D. C. and Lam, P. J.: Cycling of lithogenic marine particles in the US GEOTRACES North Atlantic
712 transect, *Deep. Res. Part II Top. Stud. Oceanogr.*, 116, 283–302, doi:10.1016/j.dsr2.2014.11.019, 2015.

713 Peers, G. and Price, N. M.: A role for manganese in superoxide dismutases and growth of iron-deficient diatoms,
714 *Limnol. Oceanogr.*, 49(5), 1774–1783, doi:10.4319/lm.2004.49.5.1774, 2004.

715 Planquette, H. and Sherrell, R. M.: Sampling for particulate trace element determination using water sampling
716 bottles: Methodology and comparison to in situ pumps, *Limnol. Oceanogr. Methods*, 10(5), 367–388,
717 doi:10.4319/lom.2012.10.367, 2012.

718 Planquette, H., Fones, G. R., Statham, P. J. and Morris, P. J.: Origin of iron and aluminium in large particles (>
719 53 μm) in the Crozet region, Southern Ocean, *Mar. Chem.*, 115(1–2), 31–42, doi:10.1016/j.marchem.2009.06.002,
720 2009.

721 Planquette, H., Sanders, R. R., Statham, P. J., Morris, P. J. and Fones, G. R.: Fluxes of particulate iron from the
722 upper ocean around the Crozet Islands: A naturally iron-fertilized environment in the Southern Ocean, *Global*
723 *Biogeochem. Cycles*, 25(2), doi:10.1029/2010GB003789, 2011.

724 Planquette, H., Sherrell, R. M., Stammerjohn, S. and Field, M. P.: Particulate iron delivery to the water column
725 of the Amundsen Sea, Antarctica, *Mar. Chem.*, 153, 15–30, doi:10.1016/j.marchem.2013.04.006, 2013.

726 Radic, A., Lacan, F. and Murray, J. W.: Iron isotopes in the seawater of the equatorial Pacific Ocean: New
727 constraints for the oceanic iron cycle, *Earth Planet. Sci. Lett.*, 306(1–2), 1–10, doi:10.1016/j.epsl.2011.03.015,
728 2011.

729 Raiswell, R., Benning, L. G., Tranter, M. and Tulaczyk, S.: Bioavailable iron in the Southern Ocean: The
730 significance of the iceberg conveyor belt, *Geochem. Trans.*, 9(1), 7, doi:10.1186/1467-4866-9-7, 2008.

731 Rijkenberg, M. J. A., Middag, R., Laan, P., Gerringa, L. J. A., Van Aken, H. M., Schoemann, V., De Jong, J. T.
732 M. and De Baar, H. J. W.: The distribution of dissolved iron in the West Atlantic Ocean, PLoS One, 9(6), 1–14,
733 doi:10.1371/journal.pone.0101323, 2014.

734 Sanders, R., Henson, S. A., Koski, M., De La Rocha, C. L., Painter, S. C., Poulton, A. J., Riley, J., Salihoglu, B.,
735 Visser, A., Yool, A., Bellerby, R. and Martin, A. P.: The Biological Carbon Pump in the North Atlantic, Prog.
736 Oceanogr., 129(PB), 200–218, doi:10.1016/j.pocean.2014.05.005, 2014.

737 Sarthou, G., Lherminier, and the GEOVIDE team: Introduction to the French GEOTRACES North Atlantic
738 Transect (GA01): GEOVIDE cruise, Biogeosciences, 15, 7097–7109, <https://doi.org/10.5194/bg-15-7097-2018>,
739 2018.

740 Sarthou, G., Vincent, D., Christaki, U., Obernosterer, I., Timmermans, K. R. and Brussaard, C. P. D.: The fate of
741 biogenic iron during a phytoplankton bloom induced by natural fertilisation: Impact of copepod grazing, Deep.
742 Res. Part II Top. Stud. Oceanogr., 55(5–7), 734–751, doi:10.1016/j.dsr2.2007.12.033, 2008.

743 Schlosser, C., Schmidt, K., Aquilina, A., Homoky, W. B., Castrillejo, M., Mills, R. A., Patey, M. D., Fielding, S.,
744 Atkinson, A. and Achterberg, E. P.: Mechanisms of dissolved and labile particulate iron supply to shelf waters
745 and phytoplankton blooms off South Georgia, Southern Ocean, Biogeosciences, 15, 4973–4993, doi: 10.5194/bg-
746 15-4973-2018, 2018.

747 Shelley, R. U., Landing, W. M., Ussher, S. J., Planquett, H. and Sarthou, G.: Characterisation of aerosol
748 provenance from the fractional solubility of Fe (Al, Ti, Mn, Co, Ni, Cu, Zn, Cd and Pb) in North Atlantic aerosols
749 (GEOTRACES GA01 and GA03), Biogeosciences, 15, 2271–2288, doi: 10.5194/bg-15-2271-2018, 2018

750 Shelley, R. U., Landing, W. M., Ussher, S. J., Planquette, H. and Sarthou, G.: Regional trends in the fractional
751 solubility of Fe and other metals from North Atlantic aerosols (GEOTRACES cruises GA01 and GA03) following
752 a two-stage leach, Biogeosciences, 15(1), 2271–2288, doi:10.5194/bg-15-2271-2018, 2018.

753 Sherrell, R. M., Field, P. M. and Gao, Y.: Temporal variability of suspended mass and composition in the
754 Northeast Pacific water column: Relationships to sinking flux and lateral advection, Deep. Res. Part II Top. Stud.
755 Oceanogr., 45(4–5), 733–761, doi:10.1016/S0967-0645(97)00100-8, 1998.

756 Spinrad, R. W., Zaneveld, J. R. and Kitchen, J.C.: A Study of the Optical Characteristics of the Suspended Particles
757 Benthic Nepheloid Layer of the Scotian Rise, J. Geophys. Res., 88, 7641–7645, doi:10.1029/83J003C, 1983.

758 Statham, P. J., Skidmore, M. and Tranter, M.: Inputs of glacially derived dissolved and colloidal iron to the coastal
759 ocean and implications for primary productivity, Global Biogeochem. Cycles, 22(3), 1–11,
760 doi:10.1029/2007GB003106, 2008.

761 Straneo, F., Pickart, R. S. and Lavender, K.: Spreading of Labrador sea water: An advective-diffusive study based
762 on Lagrangian data, Deep. Res. Part I Oceanogr. Res. Pap., 50(6), 701–719, doi:10.1016/S0967-0637(03)00057-
763 8, 2003.

- 764 Sunda, W. G. and Huntsman, S. A.: Effect of Competitive Interactions Between Manganese and Copper on
765 Cellular Manganese and Growth in Estuarine and Oceanic Species of the Diatom *Thalassiosira*, *Limnol.*
766 *Oceanogr.*, 28(5), 924–934, doi:10.4319/lo.1983.28.5.0924, 1983.
- 767 Tagliabue, A., Bopp, L., Dutay, J. C., Bowie, A. R., Chever, F., Jean-Baptiste, P., Bucciarelli, E., Lannuzel, D.,
768 Remenyi, T., Sarthou, G., Aumont, O., Gehlen, M. and Jeandel, C.: Hydrothermal contribution to the oceanic
769 dissolved iron inventory, *Nat. Geosci.*, 3(4), 252–256, doi:10.1038/ngeo818, 2010.
- 770 Tagliabue, A., Bowie, A. R., Boyd, P. W., Buck, K. N., Johnson, K. S. and Saito, M. A.: The integral role of iron
771 in ocean biogeochemistry, *Nature*, 543(7643), 51–59, doi:10.1038/nature21058, 2017.
- 772 Taylor, S. and McLennan, S.: The geochemical evolution of the continental crust, *Rev. Geophys.*, 33(2), 241–
773 265, doi:10.1029/95RG00262, 1995.
- 774 Tebo, B. M. and Emerson, S. R.: Effect of Oxygen Tension Manganese (II) Concentration and Temperature on
775 the Microbially Catalyzed Manganese-Ii Oxidation Rate in a Marine Fjord, *Appl. Environ. Microbiol.*, 50(5),
776 1268–1273, 1985.
- 777 Tebo, B. M., Neelson, K. H., Emerson, S. and Jacobs, L.: Microbial mediation of Mn(II) and Co(II) precipitation
778 at the o₂/H₂S interfaces in two anoxic fjords, 29(6), 1247–1258, 1984.
- 779 Tonnard, M., Planquette, H., Bowie, A. R., van der Merwe, P., Gallinari, M., Desprez de Gésincourt, F., Germain,
780 Y., Gourain, A., Benetti, M., Reverdin, G., Tréguer, P., Boutorh, J., Cheize, M., Menzel Barraqueta, J.L., Pereira-
781 Contreira, L., Shelley, R., Lherminier, P., and Sarthou, G.: Dissolved iron in the North Atlantic Ocean and
782 Labrador Sea along the GEOVIDE section (GEOTRACES section GA01), *Biogeosciences Discuss.*,
783 <https://doi.org/10.5194/bg-2018-147>, 2018
- 784 Trefry, J. H., Trocine, R. P., Klinkhammer, G. P. and Rona, P. A.: Iron and copper enrichment of suspended
785 particles in dispersed hydrothermal plumes along the mid-Atlantic Ridge, *Geophys. Res. Lett.*, 12(8), 506–509,
786 doi:10.1029/GL012i008p00506, 1985.
- 787 Ussher, S. J., Achterberg, E. P. and Worsfold, P. J.: Marine biogeochemistry of iron, *Environ. Chem.*, 1(2), 67–
788 80, doi:10.1071/EN04053, 2004.
- 789 Ussher, S. J., Worsfold, P. J., Achterberg, E. P., Laëis, A., Blain, S., Laan, P., de Baar, H. J. W.: Distribution and
790 redox speciation of dissolved iron on the European continental margin, *Limnol. Oceanogr.*, 52(6), 2530–2539,
791 doi:10.4319/lo.2007.52.6.2530, 2007.
- 792 Van der Merwe, P., Lannuzel, D., Bowie, A. R., Mancuso Nichols, C. A. and Meiners, K. M.: Iron fractionation
793 in pack and fast ice in East Antarctica: Temporal decoupling between the release of dissolved and particulate iron
794 during spring melt, *Deep. Res. Part II Top. Stud. Oceanogr.*, 58(9–10), 1222–1236,
795 doi:10.1016/j.dsr2.2010.10.036, 2011a.

796 Van Der Merwe, P., Lannuzel, D., Bowie, A. R. and Meiners, K. M.: High temporal resolution observations of
797 spring fast ice melt and seawater iron enrichment in East Antarctica, *J. Geophys. Res. Biogeosciences*, 116(3), 1–
798 18, doi:10.1029/2010JG001628, 2011b.

799 Weinstein, S. E. and Moran, S. B.: Distribution of size-fractionated particulate trace metals collected by bottles
800 and in-situ pumps in the Gulf of Maine-Scotian Shelf and Labrador Sea, *Mar. Chem.*, 87(3–4), 121–135,
801 doi:10.1016/j.marchem.2004.02.004, 2004.

802 Yashayaev, I.: Hydrographic changes in the Labrador Sea, 1960-2005, *Prog. Oceanogr.*, 73(3–4), 242–276,
803 doi:10.1016/j.pocean.2007.04.015, 2007.

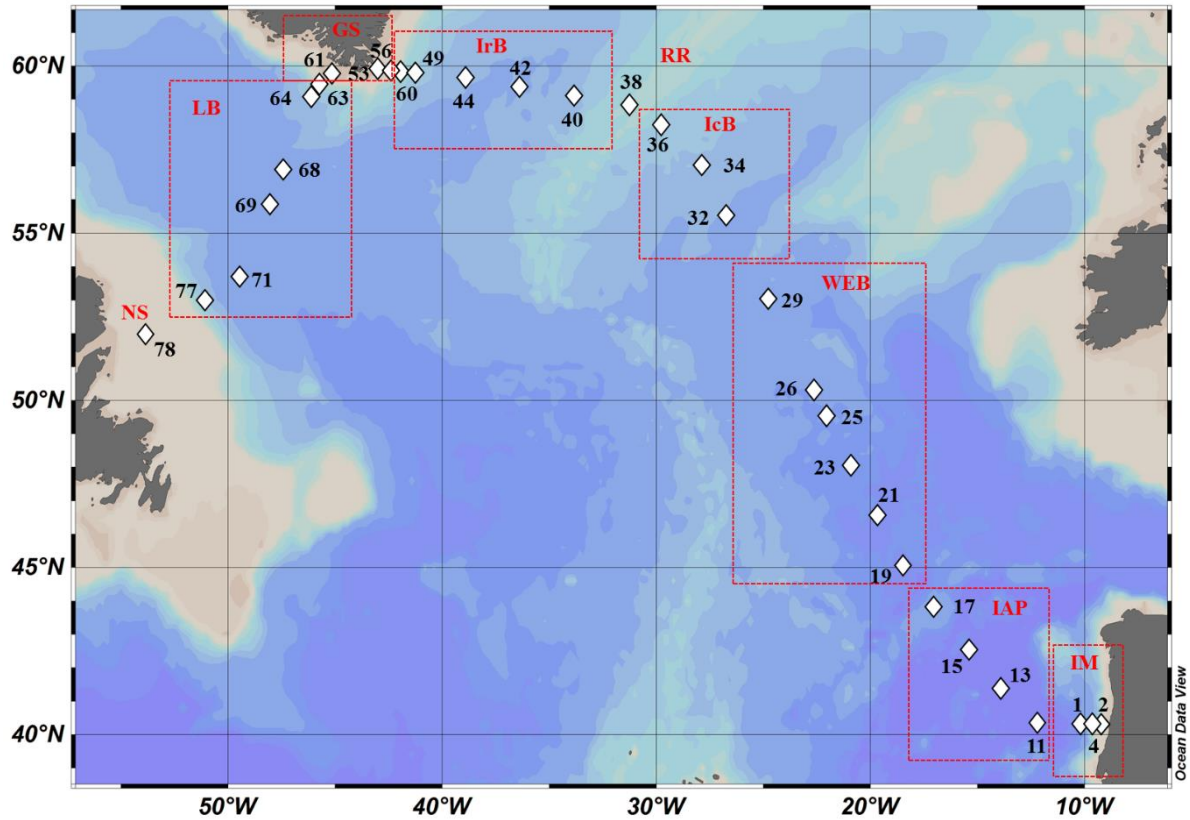
804 Yashayaev, I. and Loder, J. W.: Enhanced production of Labrador Sea Water in 2008, *Geophys. Res. Lett.*, 36(1),
805 doi:10.1029/2008GL036162, 2009.

806 Zunino, P., Lherminier, P., Mercier, H., Danialt, N., García-Ibáñez, M. I., and Pérez, F. F.: The GEOVIDE
807 cruise in May–June 2014 reveals an intense Meridional Overturning Circulation over a cold and fresh subpolar
808 North Atlantic. *Biogeosciences*, 14(23), 5323, 2017.

809
810
811
812
813
814
815
816
817
818
819
820
821
822
823
824
825
826
827
828
829
830
831
832
833

834
835
836
837
838
839
840
841

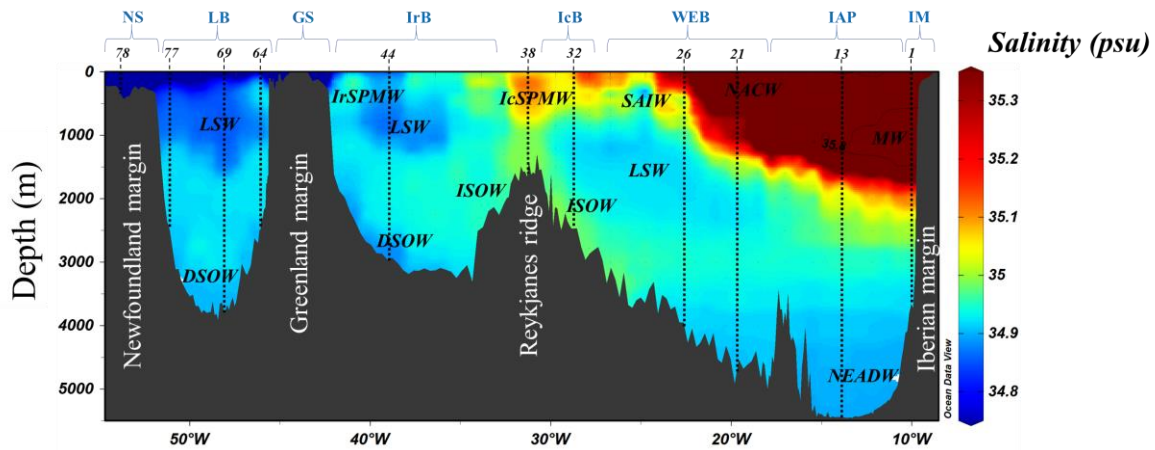
Figure 1: Map of stations where suspended particle samples were collected with GO-FLO bottles during the GEOVIDE cruise (GA01) in the North Atlantic Ocean. Biogeochemical provinces are indicated by red squares, IM: Iberian Margin, IAP: Iberian Abyssal Plain, WEB: Western European Basin, IcB: Iceland Basin, RR: Reykjanes Ridge, IrB: Irminger Basin, GS: Greenland Shelf, LB: Labrador Basin, NS: Newfoundland Shelf. This figure was generated using Ocean Data View (Schlitzer, R., Ocean Data View, odv.awi.de, 2017).



842
843
844
845
846
847
848
849
850
851
852
853
854
855

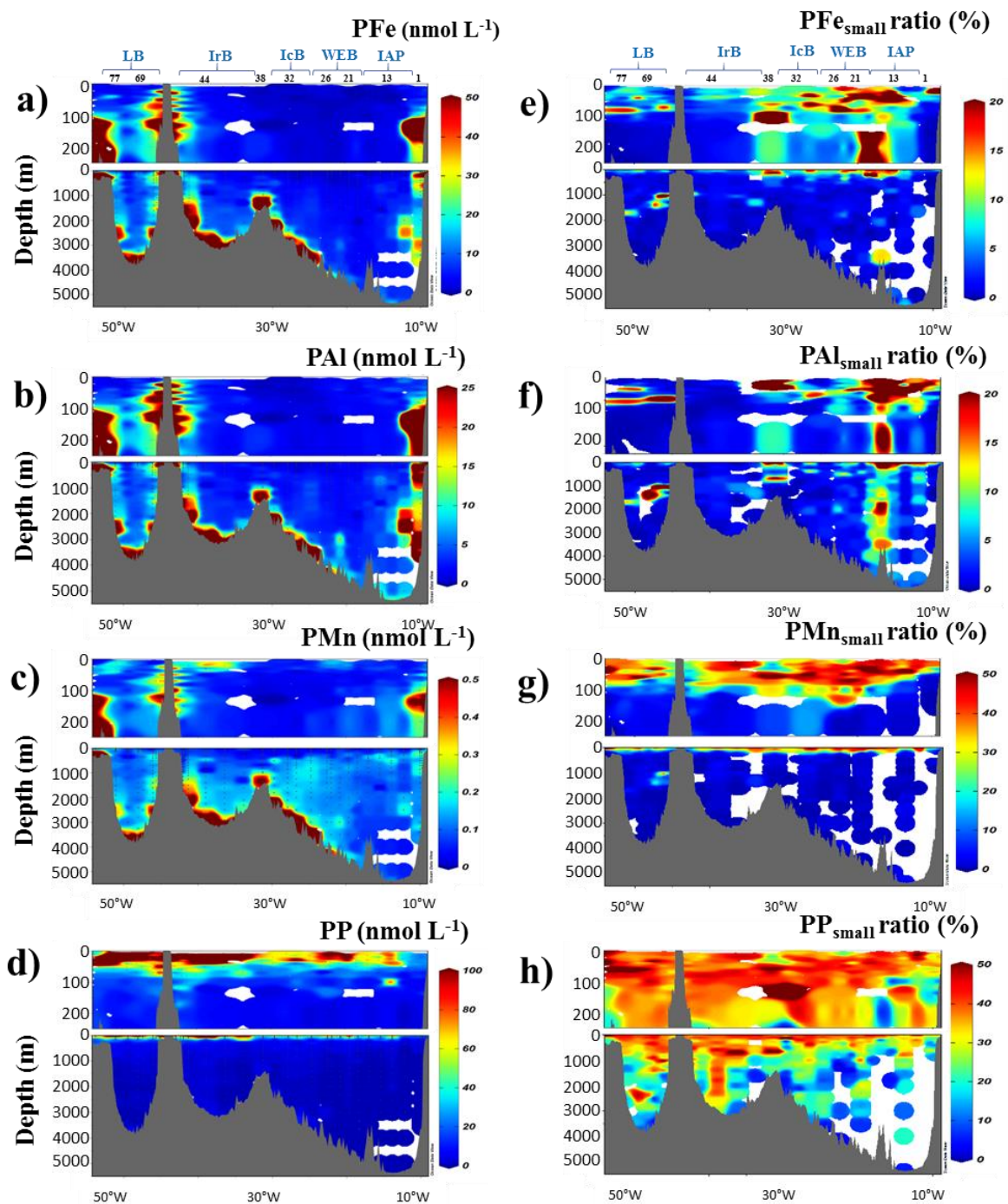
856
 857
 858
 859
 860
 861
 862
 863
 864
 865
 866
 867
 868
 869
 870
 871
 872
 873
 874
 875
 876
 877
 878
 879
 880
 881
 882
 883
 884
 885

Figure 2: Salinity section during the GEOVIDE cruise with water masses indicated in black italic font. A salinity contour of 35.8 psu have been applied to identify the Mediterranean Water (MW) to the east. From right to left; North East Atlantic Deep Water (NEADW); North Atlantic Central Water (NACW); Labrador Sea Water (LSW); Sub-Arctic Intermediate Water (SAIW); Iceland-Scotland Overflow Water (ISOW); Iceland Sub-Polar Mode Water (IcSPMW); Denmark Strait Overflow Water (DSOW); Irminger Sub-Polar Mode Water (IrSPMW). Station locations are indicated by the numbers above the section and biogeochemical provinces are indicated in blue font above station numbers. This figure was generated using Ocean Data View (Schlitzer, R., Ocean Data View, odv.awi.de, 2017).



886
887

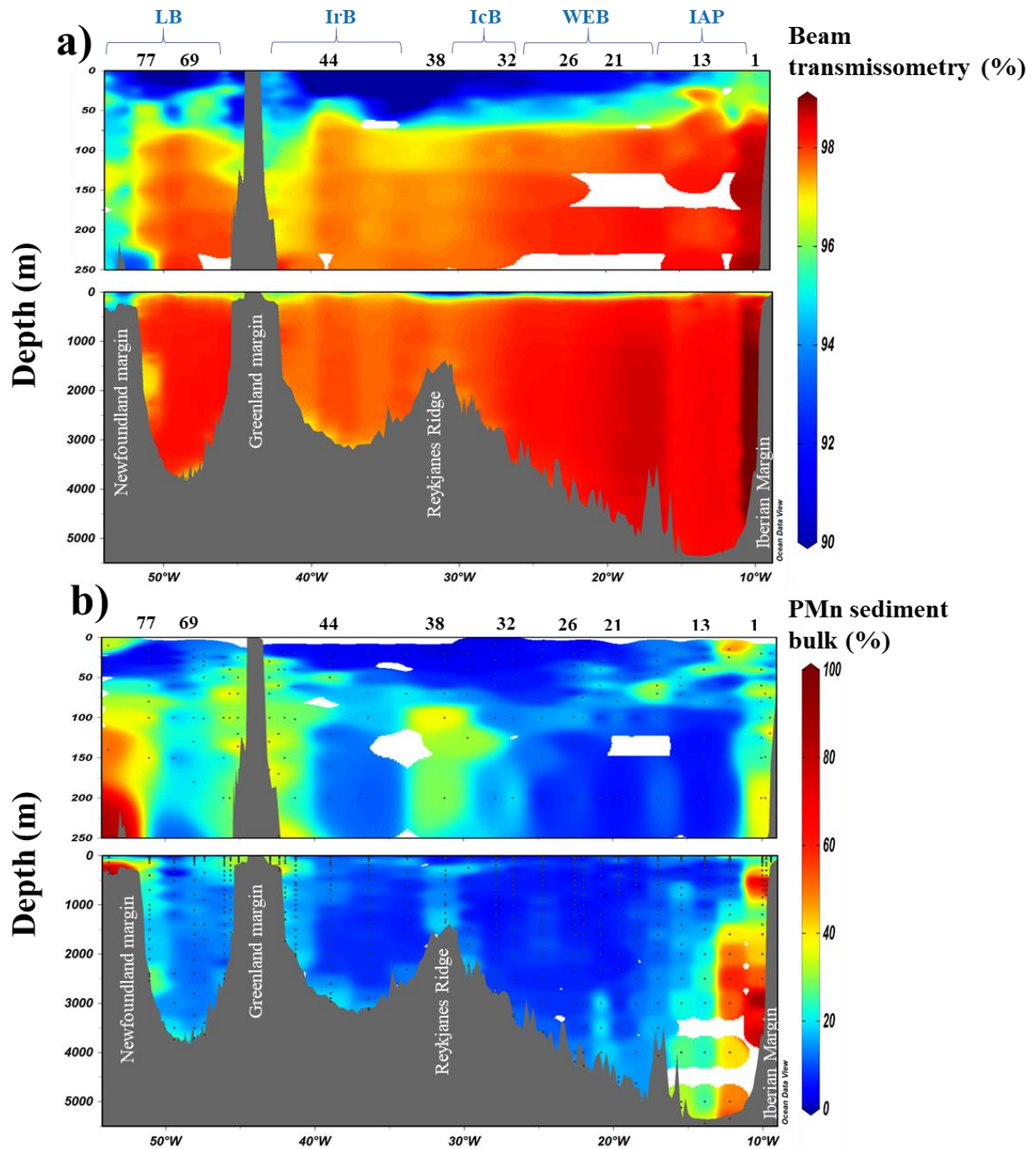
888 **Figure 3:** Left panel: Distribution of total particulate (a) iron (PFe), (b) aluminium (PAI), (c) manganese (PMn) and
889 (d) phosphorus (PP) concentrations (nmol L^{-1}) in the first 250 m and the entire water column along the GEOVIDE
890 section in the North Atlantic Ocean. Right panel: Contribution of the small size fraction ($0.45\text{-}5\ \mu\text{m}$) expressed as a
891 percentage (%) of the total concentration of (e) PFe, (f) PAI, (g) PMn and (h) PP. Station IDs and biogeochemical
892 regions are indicated on top of sections a and e. This figure was generated using Ocean Data View (Schlitzer, R., Ocean
893 Data View, odv.awi.de, 2017).



894
895
896

897

898 **Figure 4:** Section of derived contributions of sedimentary inputs along the GA01 section with (a) beam transmissometry
899 (%) and (b) manganese bulk sediment proxy (%) based on Eq (3). Station IDs and biogeochemical region are indicated
900 above section (a) in black numbers and blue letters, respectively. This figure was generated using Ocean Data View
901 (Schlitzer, R., Ocean Data View, odv.awi.de, 2017).



902

903

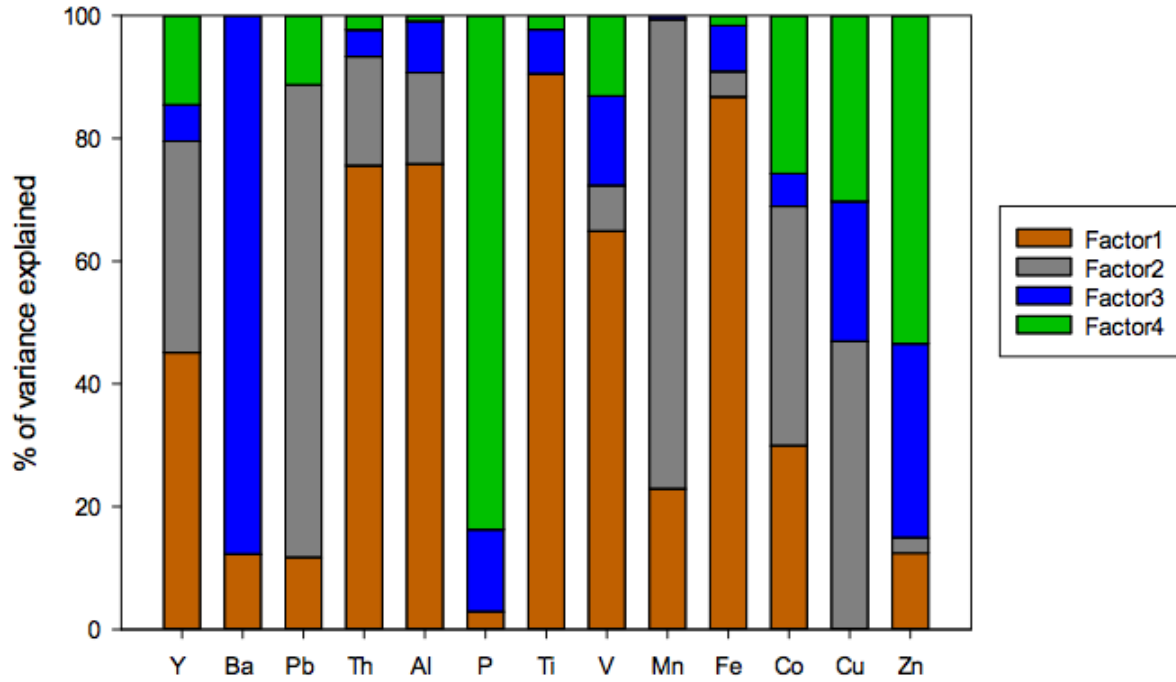
904

905

906

907

908 **Figure 5: Factor fingerprint of the positive matrix factorisation conducted on 445 particles samples collected along the**
909 **GA01 section. The four main factors influencing the particulate trace element variance are represented in a stacked**
910 **bar chart of the percentage of variance explained per element. Factor 1 is dominated by the lithogenic elements, e.g.**
911 **Th, Al, Ti and Fe. Factor 2 is associated with Pb and Mn variances. Biogenic barite formation mainly influences factor**
912 **3. Factor 4 is dominated by biogenic elements, e.g. P, Co, Cu and Zn.**



913

914

915

916

917

918

919

920

921

922

923

924

925

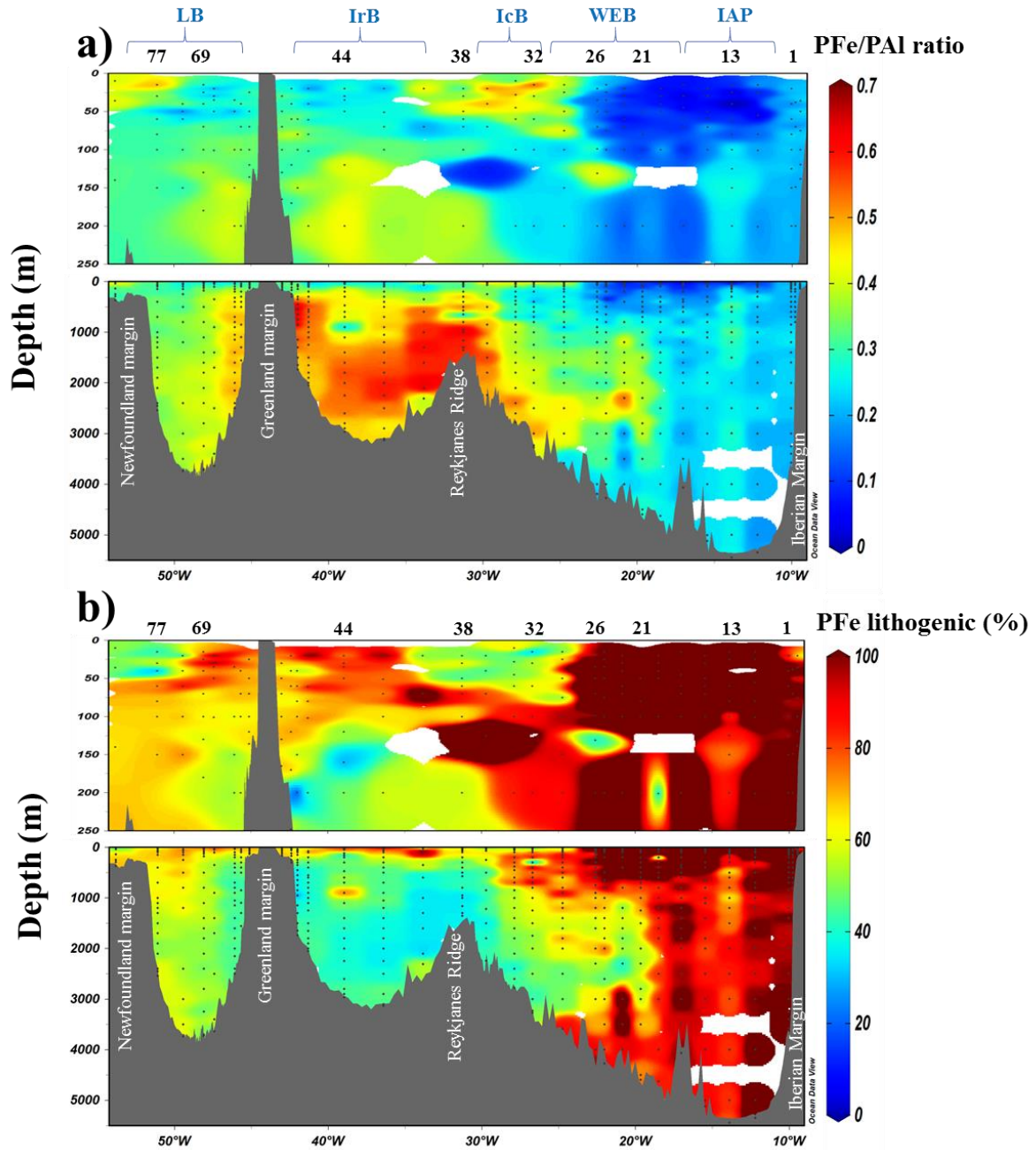
926

927

928

929

930 **Figure 6:** a) Section of the PFe to PAI molar ratio (mol mol^{-1}) during the GEOVIDE cruise (GA01) and (b) contribution
931 (%) of lithogenic particulate iron ($\text{PFe}_{\text{litho}}$) based on Eq. (1). Station IDs and biogeochemical provinces are indicated
932 above each section in black numbers and blue letters, respectively. This figure was generated using Ocean Data View
933 (Schlitzer, R., Ocean Data View, odv.awi.de, 2017).



934

935

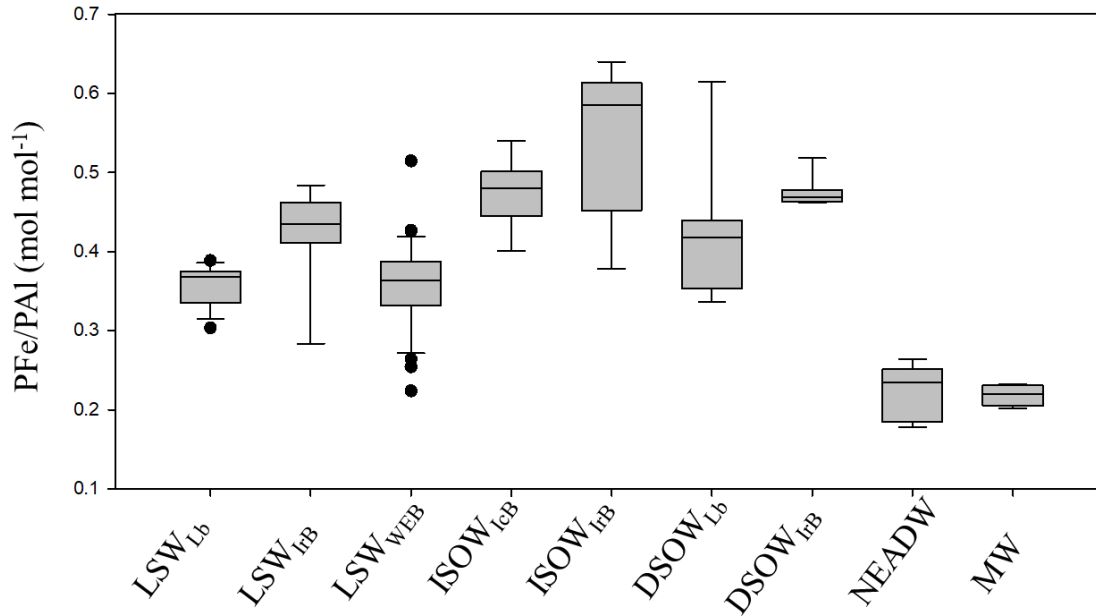
936

937

938

939

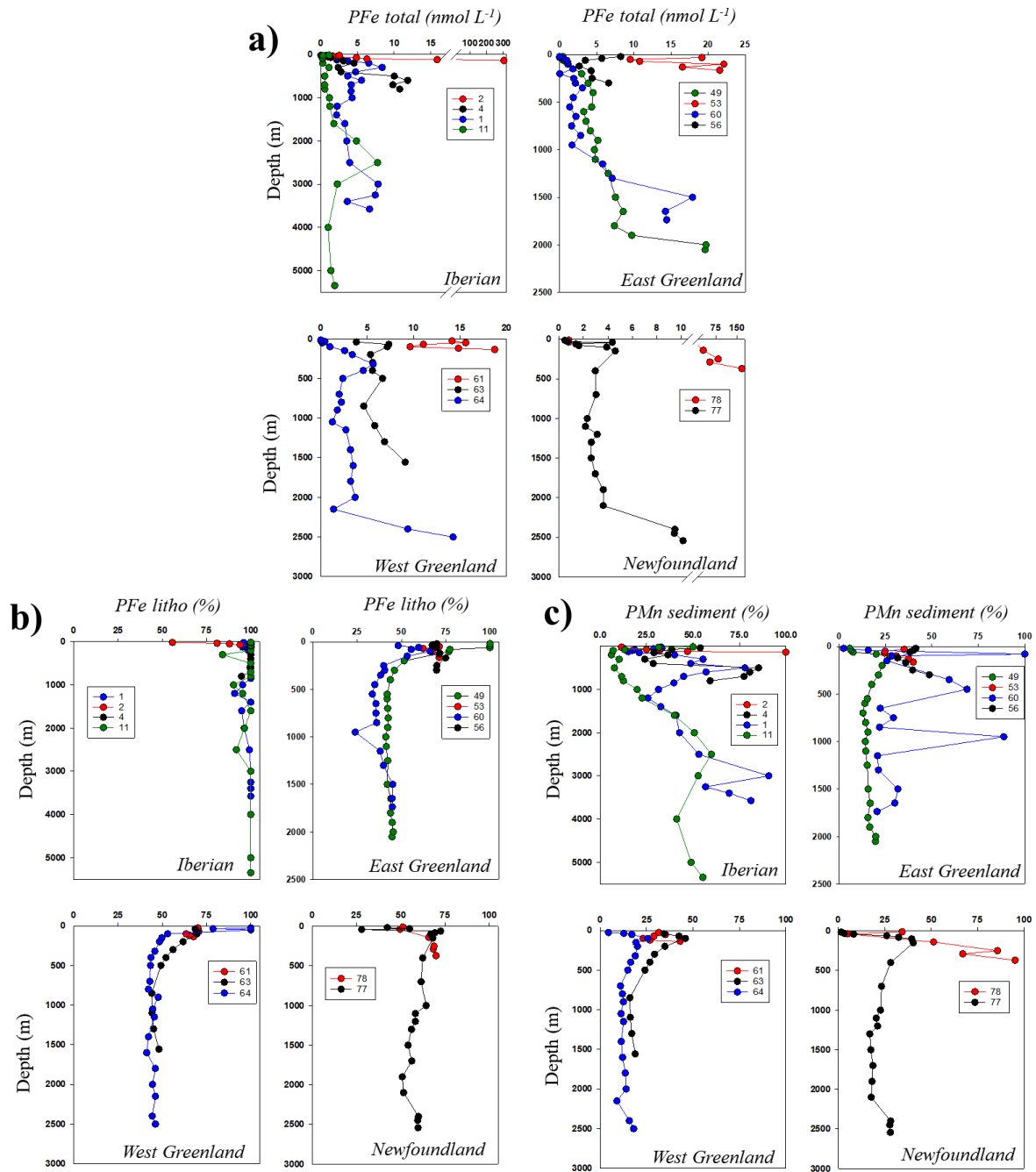
940 **Figure 7: Box and whisker diagram of PFe/PAI molar ratio in nine water masses sampled along the GA01 section in**
 941 **the North Atlantic Ocean. Water masses are defined in section 3.1 and in Figure 2. The PFe/PAI median values for each**
 942 **water masses with the biogeochemical provinces in subscript were as follows: LSW_{LB} = 0.37; LSW_{IFB} = 0.44; LSW_{WEB}**
 943 **= 0.36; ISOW_{ICB} = 0.48; ISOW_{IFB} = 0.58; DSOW_{LB} = 0.42; DSOW_{IFB} = 0.47; NEADW_{IAP} = 0.23; MW = 0.22 mol mol⁻¹.**
 944 **The difference in PFe/PAI between water masses is statistically significant (Kruskal-Wallis test; p = < 0.001 excluding**
 945 **water masses for which we had less than 5 data points for PFe/PAI). Noted that the UCC PFe/PAI ratio reported from**
 946 **Taylor and McLennan, (1995) is 0.21 mol mol⁻¹.**
 947



948
 949
 950
 951
 952
 953
 954
 955
 956
 957
 958
 959
 960
 961
 962
 963
 964

965
966
967

Figure 8: Vertical profiles of (a) PFe (nmol L⁻¹), (b) lithogenic proportion of particulate iron (PFe_{litho}, %) and (c) sedimentary proportion of particulate manganese (PMn sediment, %) at the Iberian, East-West Greenland and Newfoundland margins.



968

969

970

971

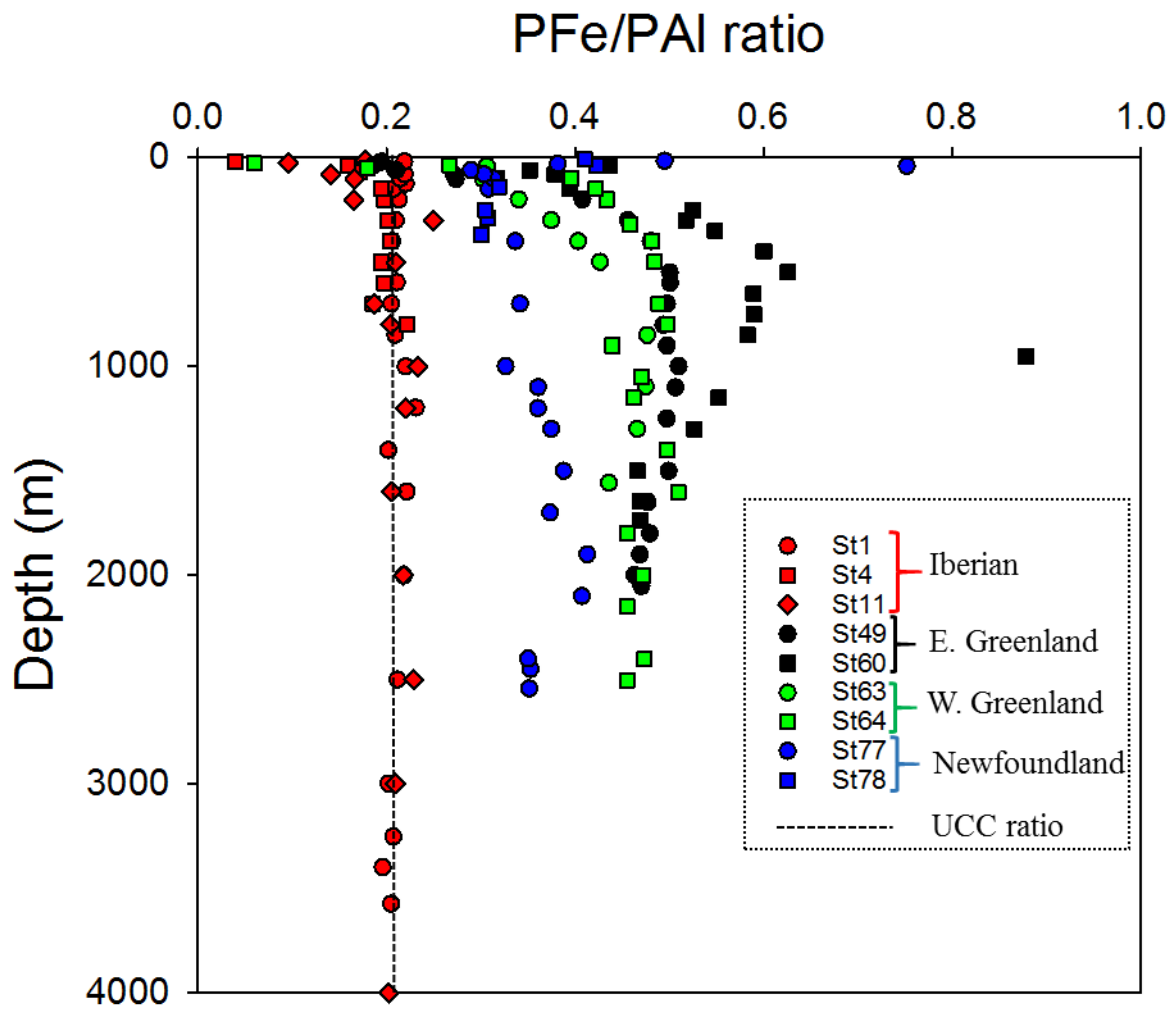
972

973

974

975
976
977

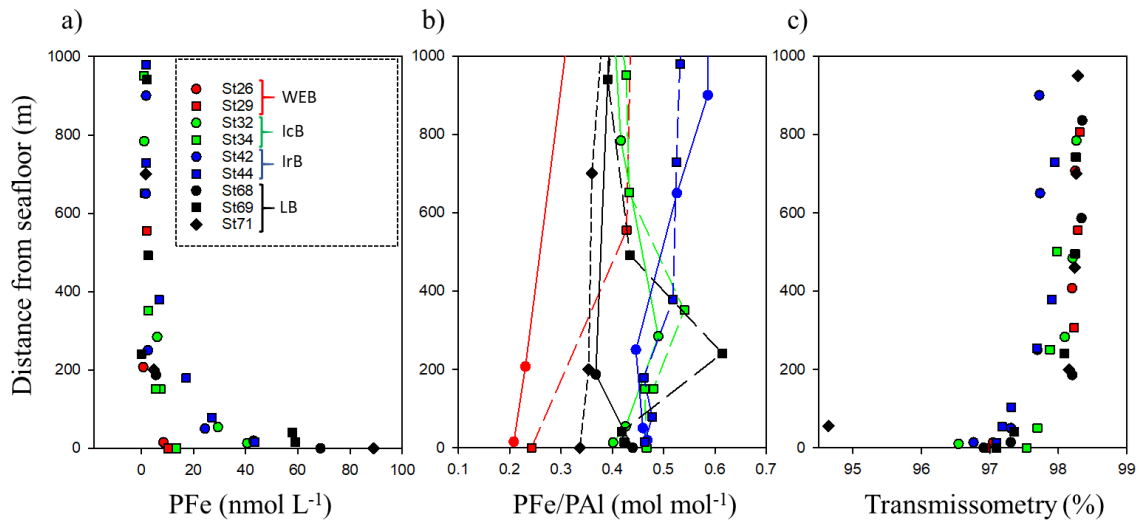
Figure 9: Scatter of the PFe/PAI ratio at the Iberian (red dots), East Greenland (black dots), West Greenland (green dots) and Newfoundland margins (blue dots). Dashed line indicate the UCC PFe/PAI ratio (Taylor and McLennan, 1995).



978
979
980
981
982
983
984
985
986
987
988

989 **Figure 10: Benthic Nepheloid Layers (BNLs) encountered along the GA01 section and observed through a) PFe total;**
 990 **b) PFe/PAI ratio and c) beam transmissometry (%) as a function of depth above the seafloor (m) at selected stations**
 991 **where a decrease in transmissometry was recorded in the West European (red dots), the Iceland (green dots), the**
 992 **Irminger (blue dots) and the Labrador Basins. Noted that the UCC PFe/PAI ratio reported from Taylor and McLennan,**
 993 **(1995) is 0.21 mol mol⁻¹.**

994



995

996

997

998

999

1000

1001

1002

1003

1004

1005

1006

1007

1008

1009

1010

1011

1012

		Fe	Al	P	Mn
Blank (nmol L ⁻¹)	5µm filter	0.072	0.100	0.511	0.003
	0.45µm filter	0.132	0.164	1.454	0.005
Limit of detection (nmol L ⁻¹)	5µm filter	0.011	0.030	0.365	0.001
	0.45µm filter	0.026	0.046	1.190	0.001
Recovery CRM (%)	BCR-414 (n=10)	88 ± 7			94 ± 7
	MESS-4 (n=5)	98 ± 14	97 ± 14	80 ± 30	110 ± 18
	PACS-3 (n=8)	101 ± 9	99 ± 14	91 ± 34	112 ± 11

1013

1014

Table 1: Blank and limit of detection (nmol L⁻¹) of the two filters and certified reference material (CRM) recoveries during GEOVIDE suspended particle digestions.

1015

1016

1017

1018

1019

Location	Depth range	PFe	PAI	PMn	PP	Fraction	Author	Year
N. Atlantic (>40°N)	All	bdl-304	bdl-1544	bdl-3.5	bdl-402	>0.45µm	This study	
Labrador Sea	0-250	0.1-1.2	0.1-1.5			>53 µm	Weinstein et al.	2004
Labrador Sea	0-250	2.5	3.6	0.05		0.4– 10µm	Weinstein et al.	2004
N. Atlantic (25-60°N)	Upper 1000m	0.29-1.71	0.2-19.7			0.4µm	Barrett et al.	2012
N. Atlantic	All	0-938	0-3600			0.8–51 µm	Ohnemus et al.	2015
Gulf of Maine	0-300	34.8	109			>0.4 µm	Weinstein et al.	2004
Eastern tropical N.A.	0-200		0.59-17.7			>0.2 µm	Dammshausser et al.	2013
Eastern tropical N.A.	0-600	ND-12				1–51 µm	Lam et al.	2012
Sub-tropical N.A.	All	ND-140	ND-800			>0.45µm	Milne et al.	2017
Meridional Atlantic	0-200		0.35-16.1			>0.2 µm	Dammshausser et al.	2013
Northeast Pacific	0-3557		0.0-54.2			1-53µm	Sherrell et al.	1998
Eastern tropical S.Pacific	All	bdl-159	bdl-162	bdl-8.7	bdl-983	>0.8 µm	Lee et al.	2017
South Georgia Shelf	All	0.87-267	0.6-195	0.01-3.85		>1 µm	Schlosser et al.	2017
Southern Ocean	30-340	0.15–13.2	0.11–25.5			>53 µm	Planquette et al.	2009
East Antarctic	Surface		0.02-10.67	0.01-0.14		>0.2 µm	Lannuzel et al.	2011
East Antarctic	Fast ice	43-10385	121-31372	1-307		>0.2 µm	Lannuzel et al.	2014
Ross Sea	All	0.68-57.3	ND-185	ND-1.4	5.4-404	>0.4 µm	Marsay et al.	2017

1020

1021

Table 2: Concentration (in nmol L⁻¹) of particulate trace elements (PFe, PAI, PMn and PP) in suspended particles collected in diverse regions of the world's ocean. Bdl: below detection limit, ND: non-determined.

1022

1023

1024

1025